ÉCOLE POLYTECHNIQUE
FÉDÉRALE DE LAUSANNE

Swiss Federal Institute of Technology
in Lausanne, Switzerland

European Organization for
Nuclear Research, Geneva,
Switzerland

MASTER THESIS

Observations and measurements of dynamic effects due to beam-beam interactions in the LHC and extrapolation to the FCC-hh

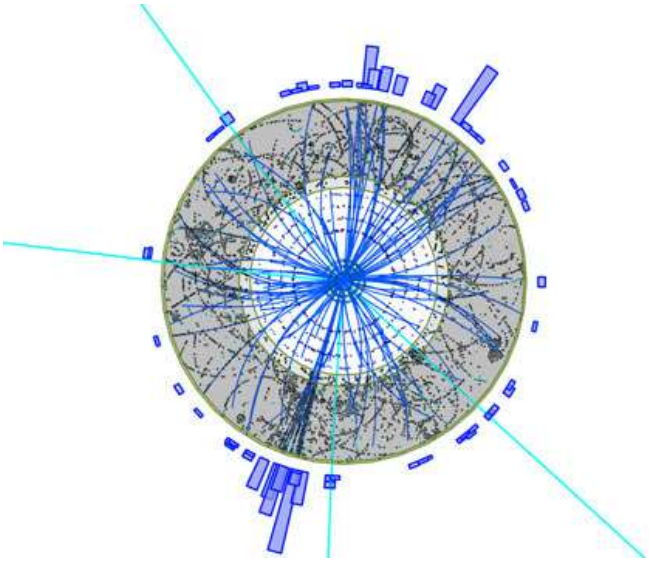

Author:
Patrik GONÇALVES JORGE

Supervisor:
Dr. Javier BARRANCO
Director:
Prof. Leonid RIVKIN

August 22, 2017

Contents

Acknowledgements

I would like to acknowledge the people that contributed to this work. They not only supported me during this master thesis but also made my stay enjoyable and fruitful.

In particular, I would like to thank my supervisor, Javier Barranco, for the time he spent mentoring me and teaching me. He was always present whenever I needed and pushed me to do my best.

Xavier and Tatiana were never far away and they were always ready to answer my questions. Their enthusiasm and ideas for new studies were really inspiring. Claudia and Laurent helped me several times regarding the simulation code I was introduced to.

I would like to particularly thank Lenny Rivkin. He gave me the opportunity to enter the world of accelerator physics in the frame of laboratory work during my master studies at EPFL and then to realize this master thesis. He also supported my work by financing computing time on EPFL's clusters.

The people from the optics team have been extremely supportive. Felix, Jaime and Elena provided all the tools to compute the optics from the experimental data. I would like to acknowledge also Rogelio Tomás for the analytical support he provided to this master thesis in Sec. 3.

The help from the EPFL's High Performance Computing team was precious. They were always present to give advice and help for the clusters.

Finally, during this master thesis, the collaboration I had with the people at CERN made me feel like I was a colleague more than a student. This experience was truly enriching from a scientific point of view, rewarding and I acquired valuable experience. I had the opportunity to write a MD note [1], a paper for IPAC conference [2], to create a poster for this conference and also to contribute to a scientific paper [3].

Abstract

The Future Circular hadron-hadron Collider (FCC-hh) is a design study for a 100 TeV centre-of-mass energy. The dynamics of the beams in such a collider poses many challenges, in particular the amount of energy stored in each beam (8.4 GJ) makes them very destructive and therefore requires a tight control of the machine and beam parameters during the full cycle in order to avoid damages and reach the collider designed performances. The FCC-hh features an increase of the beam brightness during the cycle due to the presence of synchrotron radiation damping at high energy. As a result, the electromagnetic forces that the two beams exert on each other, the so-called beam-beam forces, are enhanced and might become an issue for the safe operation of the machine. In this new regime, the impact of the beam-beam interaction on the optics becomes non-negligible. In this master thesis, for the first time, the impact of the beam-beam interaction on the optics (β-beating) is measured in a hadron collider (LHC). The expected impact on luminosity and on the collimation hierarchy is addressed for the FCC-hh case.

1 Introduction

The Standard Model can be seen as a low-energy effective theory and for several phenomenological and conceptual reasons, it is believed to need some adjustments, namely the presence of new physics at high energy. The principal aim of a particle collider is to unlock this new physics by searching fundamental particles. In order to achieve this, it is necessary to have high energy particles and a high luminosity $\mathcal{L}$ since the latter is proportional to the events rate dR/dt [4]:

$$\frac{dR}{dt} = \mathcal{L} \cdot \sigma_p, \tag{1}$$

where σ_p is the cross section for a given reaction. Assuming bunches with Gaussian particle distribution, the luminosity expression can be calculated as [4]:

$$\mathcal{L} = \frac{N_1 N_2 f N_b}{4\pi\sigma_x\sigma_y}, \tag{2}$$

where N_1 and N_2 are the intensities of the bunches in beam 1 and 2 respectively, f the revolution frequency, N_b the number of bunches in one beam and $\sigma_{x,y}$ the horizontal and vertical Root Mean Square (RMS) beam size, respectively. Note that in the case of non-Gaussian beams, a numerical integration is mandatory. The ratio between the beam intensity and beam size is known as brightness. Future colliders will push to enhance the beam brightness to maximize the luminosity reach.

In a collider, two counter-rotating beams are brought into collision in one or several Interaction Points (IPs). Each beam consists in moving bunches composed of charged particles. Thus, an electromagnetic field is induced by these ensembles of moving charges. The resulting forces will affect the bunch itself (space charge effects) and the opposite beam when they meet at the IP (head-on encounter) and when they travel in a common pipe region (long range encounters). The beam-beam interactions are one of the strongest non-linearities found in the particle accelerator and lead to a variety of effects, e.g. alteration of the optics along the accelerator [5].

Since the strength of the interaction between both beams is proportional to the beams brightness, it is necessary to evaluate its impact on the optics and understand if it can be measured and corrected. For example, the RMS beam size is defined by the β-function through the accelerator : $\sigma(s) = \sqrt{\varepsilon_g \beta(s)}$ where ε_g is the geometrical emittance and s the location. Since the maximum change of the β-function due to beam-beam, i.e. the maximum of the β-beating, increases with the strength of interaction, the beams size may become too large and go beyond machine tolerances. Large or underestimated perturbations would translate into significant apertures changes along the machine leading to uncontrolled beam losses. In superconducting machines, even a small amount of losses can produce magnet quenches. Thus, this detrimental effect has to be very well understood to ensure reliable operation.

The following results and discussion will focus on two different accelerators : the Large Hadron Collider (LHC) and the Future Circular hadron-hadron Collider (FCC-hh). The LHC is the most powerful accelerator at the CERN Accelerator Complex with a 27 km circumference and a collision energy of 14 TeV [6] while the FCC-hh is a 100 km proton-proton collider design study that plans to achieve a centre-of-mass energy of 100 TeV [7]. Their general layout is presented in Fig. 1. Machine parameters of the LHC, FCC-hh and High-Luminosity LHC (HL-LHC), an upgrade of the current LHC [8], are summarized in Tab. 1.

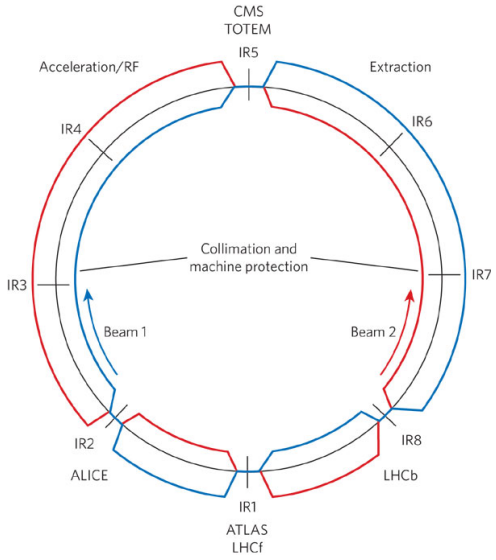

LHC [9]

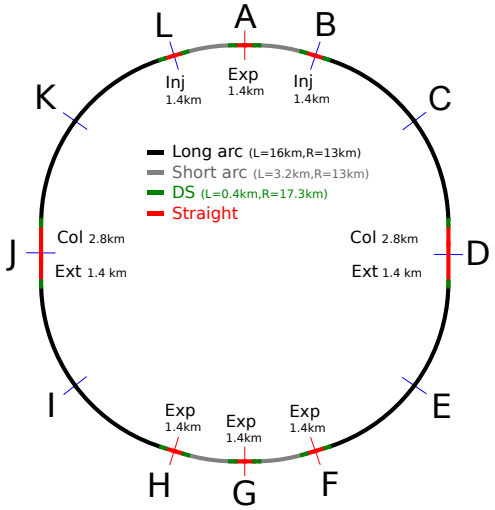

FCC-hh

Figure 1: Layout of the studied hadrons colliders

Thanks to its advanced machine and beam parameters, the FCC-hh plans to achieve a four times larger luminosity. The brightness, and thus the beam-beam effect, in the FCC-hh and in the HL-LHC is planned to be about 50% larger than in the LHC (smaller normalized emittance). As a consequence, it is crucial to evaluate the beam-beam impact on these future colliders to make sure tolerances are respected.

	LHC	**HL-LHC**	**FCC-hh**
Luminosity [10^{34}cm^{-2}s^{-1}]	1	5	20
Bunch charge [10^{11}]	1.15	2.2	1
Normalized emittance [μm]	3.75	2.5	2.2

Table 1: Machine parameters for the LHC, HL-LHC and FCC-hh [10]

In the present master thesis, the distortion of the optics due to the beam-beam interaction is addressed. Experimental data from LHC is used to understand and evaluate for the first time the β-beating due to the beam-beam interaction in a hadron collider [11, 12, 13, 14]. For this, a dedicated Machine Development (MD) study was devoted to acquire optics data while kicking the beams with the AC Dipole [15] or the Transverse Damper (ADT) [16]. Some challenges were found while performing the post-processing of the data like for example the definition of a natural tune which is a figure of merit needed to reconstruct the β-function. Computer simulations were performed to understand the observations together with analytical estimations. The optics distortion has several implications like changing the distribution shape at the IPs which will have an influence on the luminosity reach. Self-consistent simulations are done to evaluate this effect for FCC-hh. Finally, a detailed aperture model for FCC-hh is used to evaluate the impact on the aperture for different beam-beam parameters.

2 Beam-beam Interactions

The beam-beam interaction in colliders is one of the most important limits to the their performance and since LHC upgrades and future colliders will push the beam-beam interaction to new regimes, it is crucial to evaluate its impact with respect to the machine tolerances even if there exists no complete theory.

In this section, the general expression of the force from a beam acting on a particle is presented along with beam-beam concepts and variables. Then, the beam-beam collective effects and the induced coherent modes are discussed. The two codes used during the master thesis are also introduced.

2.1 Incoherent effects

The force from the electromagnetic field induced by the moving charged particle beams can be derived analytically assuming round beams and a Gaussian beam distribution. Its radial component is given by [4]:

$$F_r(r) = -\frac{nq^2(1+\beta^2)}{2\pi\epsilon_0}\frac{1}{r}\left[1-\exp\left(-\frac{r^2}{2\sigma^2}\right)\right], \tag{3}$$

where n is the line density of particles in the beam, q the elementary charge, ϵ_0 the vacuum permittivity, β corresponds here to the normalized speed of the particles and σ to the RMS beam size. The expression in Eq. 3 corresponds to the force induced by a beam and acting on a single particle. This approach is a simplified one given that the mutual self interaction between both bunches is omitted. This model is generally referred to as "weak-strong" interaction since one of the two beams is not affected. In this context, the beam-beam collision is equivalent to an electromagnetic lens that varies in time and through which the single particle is moving at the interaction point.

MAD-X [17, 18, 19] is a well-known code for optics design that allows a detailed description of the lattice and that treats the beam-beam interaction from a weak-strong point of view. The latter describes the machine by a set of elements each represented by a first or second order transfer matrix, which all together gives the one turn matrix. From the one turn matrix, the fixed points (orbit) and the eigenmodes (periodic solutions) are computed and expressed as optics (or Twiss) functions.

In Fig. 2, a comparison of the beam-beam force (Eq. 3) between beams having a different brightness is given.

For small amplitudes (i.e. for $r < 1\ \sigma$), the beam-beam force is approximately linear (Fig. 2) which means that the particle traveling sees the beam coming from the opposite direction as a defocussing quadrupole (in the case of equally charged particles). The slope of the force, which is equivalent to the kick received by the particle at the IP, increases with the beam brightness. This is why the electromagnetic field from a bright beam has a greater impact on the optics functions.

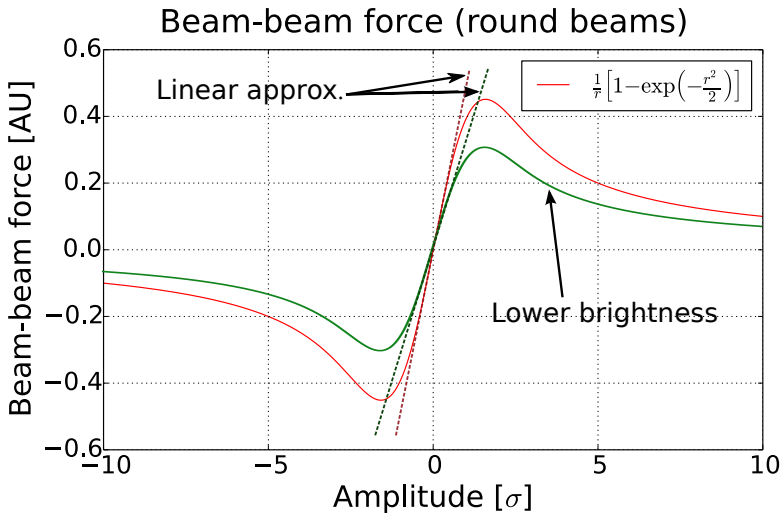

Figure 2: Beam-beam force assuming round beams (Eq. 3) showing impact of the beam brightness and with the linear approximation for small amplitudes.

The change of the β-function at the IP (β^*) under certain assumptions is known as dynamic β and can be estimated analytically [20]:

$$\frac{\beta^*}{\beta_0^*} = \frac{1}{\sqrt{1 - 4\pi\xi_{bb}\cot(2\pi Q_0) - 4\pi^2\xi_{bb}^2}}. \tag{4}$$

Eq. 4 describes the change in β at the IP due to beam-beam interaction for a zero amplitude particle with a tune Q_0 far from resonances (integer and half-integer), one IP only and a small beam-beam parameter ξ_{bb} that is defined as [4]

$$\xi_{bb} = \frac{N r_p \beta^*}{4\pi\gamma\sigma^2}, \tag{5}$$

where N corresponds to the total number of particles, r_p is the classical proton radius and γ the Lorentz factor. When one is far enough from linear resonances (half-integer and integer) and for small amplitudes ($r \to 0$), the tune shift induced by the beam-beam interaction is equal to the beam-beam parameter.

At larger amplitudes, i.e. above $\sim 1\ \sigma$, the force becomes strongly non-linear (Fig. 2). This non-linearity implies a dependency between the tune shift and the particle amplitude. The tune shift of a particle is obtained by averaging the slope of the beam-beam force over the particle's oscillation amplitude. Fig. 3 illustrates the derivative of the beam-beam force.

Given Fig. 3, the smaller is the amplitude of the particle, the larger will be its tune shift. Particles with large amplitudes have a smaller detuning due to the negative values of the derivative after $\approx 1.5\ \sigma$. Finally, for very large amplitudes, the average slope tends to zero, meaning that the tune shift becomes zero.

There are two kinds of interactions acting on the bunches of particles when they travel

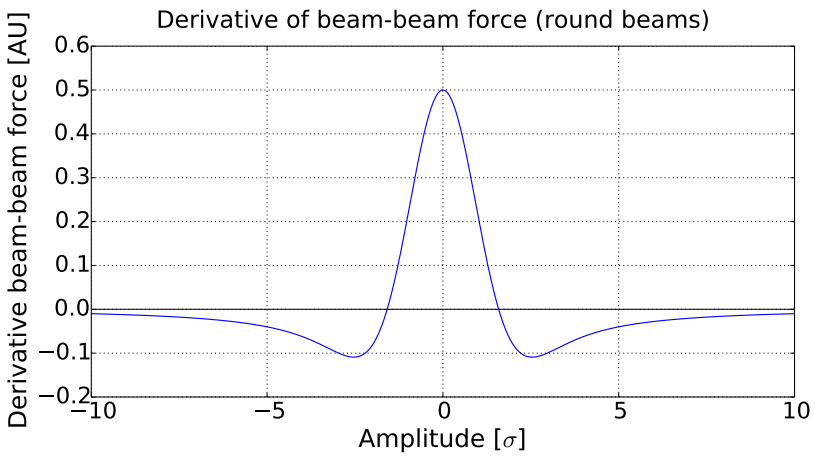

Figure 3: Derivative of the beam-beam force (Eq. 3) versus amplitude

in the same beam pipe : head-on and long-range interactions. Head-on interactions concern the interactions between bunches colliding quasi head-on at the center. The other bunches that are kept separated by the crossing angle and that feel the electromagnetic forces from the opposite beam are affected by long-range interactions. The large number of long-range interactions makes them important even if, independently, they distort the beams less than head-on collisions.

2.2 Collective effects

So far, the beam-beam interaction was presented in the case of a single particle moving through an electromagnetic lens representing the opposing beam with the assumption that the particle was not affecting the opposing beam (weak-strong regime).

However, when considering intense beams, the electromagnetic fields from the crossing bunches influence each other mutually leading to strong dynamic perturbations. These collective effects are generally related to the so-called "strong-strong" regime where the beams affect each other, contrasting with the previously defined weak-strong regime. Self-consistent beam-beam simulations where the interaction is reevaluated turn after turn using the modified beams' properties are essential to address these effects.

COherent Multi-Bunch Interaction (COMBI) is a multi-particle tracking code developed for self-consistent simulation of coherent multi-bunch beam-beam interaction [21, 22, 23]. It allows to simulate a large number of bunches undergoing a wide variety of "actions" including among others: beam-beam, impedance, transverse feedback, noise sources, collimators, synchrotron radiation.

COMBI source code was updated with a new AC dipole element during this master thesis to simulate the β-beating measurements in the LHC. This element allows to excite one of the two beams in both planes independently and perform a ramp of amplitude to ensure the adiabaticity of the process and a constant transverse beam size [24].

2.2.1 Coherent beam-beam modes

The beam-beam interaction introduces a strong coupling between both beams making the dynamics of one of the beams depend on the other and vice versa. At collision, the beam-beam force coherently excites the beams leading to a new collective motion of the beams together. The appearance of coherent modes is enhanced when we have symmetric beams optics and conditions.

This coherent motion can excite coherent dipole oscillations that correspond to oscillation of the center of mass of the bunches. This coherent motion is analog to the case of two coupled harmonic oscillators where the coupling force is the beam-beam force. In the case of a head-on interaction with a single IP and a transverse degree of freedom, two coherent modes are excited : σ-mode (in-phase oscillation of the two bunches) and π-mode (out-of-phase oscillation).

In the σ-mode, the phase difference is zero, meaning that the distance between the bunches does not change at the IP turn by turn. Therefore, there is no net force driving an oscillation and the oscillation frequency of this mode is equal to the unperturbed tune.

The π-mode corresponds to a π phase advance difference between the two bunches, leading to a maximum net force difference between two turns. Thus, the tune is modified and the new tune is $Q_0 + \Delta Q_{coh}$. Since we are dealing with particles that have equal charge, the sign of ΔQ_{coh} is negative (defocussing case). In order to calculate the factor ΔQ_{coh}, one has to solve the Vlasov equation of two coupled beams [22, 25] and use a self-consistent model of the coherent interaction because the distributions of both beams change as they interact at the IPs, leading to a different force on the individual particle (no rigid bunches). The detuning of the π-mode can be characterized relatively to the beam-beam parameter ξ_{bb} : $\Delta Q_{coh} = -Y\xi_{bb}$ where Y is the Yokoya factor [26]. In our case (COMBI simulations), the force experienced by a particle interacting with an opposing beam originates from a Gaussian distribution with variable barycenters and RMS beam sizes (soft Gaussian). The calculation of the Yokoya factor yields $Y = 1.1$ which is smaller than the one computed from models where non-Gaussian deformations of the distribution are taken into account [27].

An example of simulated spectrum from a head-on beam-beam interaction is shown in Fig. 4. The σ-mode is present at the unperturbed tune as expected. The π-mode detuning is $\sim 1.2\ \xi_{bb}$, i.e. the Yokoya factor is about 1.2 which is close to the expected value for the LHC beam characteristics (round beams at collision). The incoherent tune spread is located between these two modes and spans the interval $[0,\ \xi_{bb}]$.

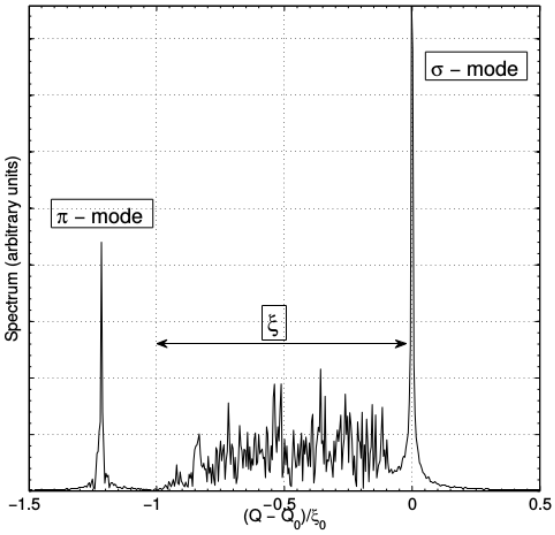

Figure 4: Relative detuning of two bunches colliding head-on from self-consistent simulation. The beam-beam coherent modes (σ and π) and the incoherent spectrum are illustrated [22].

A transverse feedback system [28] can be used during experiments to damp the coherent modes. This system stabilizes the beam by tracking its center of gravity and by kicking it back to its ideal trajectory such that the collective motion between both beams is suppressed.

3 Beam-beam amplitude detuning

Forced oscillations are often present in accelerators. In some cases they are unwanted effects like power converters ripples or noise in crab cavities that have a detrimental effect on the accelerator performance [29, 30]. In other cases like for the AC dipole (magnet with a current sinusoidally oscillated), the forced oscillations can be used to measure and control linear and non-linear dynamics [15, 24, 31]. By setting the excitation frequency near the betatron tune, it is possible to excite coherent betatron oscillations. These transverse oscillations are then used for measurements of lattice optics, rapidly diagnose errors, and study non-linear optics. The differences between free and forced oscillations are explained in [31, 32]. In [3], free and forced amplitude detuning functions are analytically derived in presence of beam-beam. The equations assume the beam-beam is an electromagnetic lens that is not changed by the opposite beam, i.e. weak-strong regime, and the beams are round with $\xi_{bb} = \xi_{bb,x} = \xi_{bb,y}$. The amplitude detuning was determined for excitations acting on a single plane (horizontal or vertical plane). We assume in what follows an horizontal excitation.

The full derivation of the amplitude detuning formulas presented next can be found in [3]. These results will be benchmarked with self-consistent simulations with COMBI in section 4 and used to better understand the measurements during the LHC experiment in section 5.

3.1 Free oscillations

The beam-beam amplitude detuning ΔQ on both planes as a function of the horizontal free excitation amplitude A_{free} in units of the RMS beam size is given by the following formulas [3]:

$$\Delta Q_x(A_{free}) = \xi_{bb} \frac{4}{A_{free}^2} \left[1 - I_0 \left(\frac{A_{free}^2}{4} \right) e^{-A_{free}^2/4} \right], \tag{6}$$

$$\Delta Q_y(A_{free}) = \xi_{bb} \left[I_0 \left(\frac{A_{free}^2}{4} \right) + I_1 \left(\frac{A_{free}^2}{4} \right) \right] e^{-A_{free}^2/4}, \tag{7}$$

where $I_n(x)$ is the modified Bessel function of the first kind. A sketch of the relative detuning versus the excitation amplitude in the case of free oscillations is given in Fig. 5a.

3.2 Forced oscillations

From the free amplitude detuning functions (Eqs. 6 and 7), one can derive the equivalent amplitude detuning functions in both transverse planes involving forced oscillations [3]:

$$\Delta Q_x(A_{forced}) = \xi_{bb}\left[I_0\left(\frac{A^2_{forced}}{4}\right) - I_1\left(\frac{A^2_{forced}}{4}\right)\right] e^{-A^2_{forced}/4}, \tag{8}$$

$$\Delta Q_y(A_{forced}) = \xi_{bb}\left[I_0\left(\frac{A^2_{forced}}{4}\right) + I_1\left(\frac{A^2_{forced}}{4}\right)\right] e^{-A^2_{forced}/4}, \tag{9}$$

where A_{forced} corresponds now to the horizontal forced excitation amplitude in units of the RMS beam size. A sketch of the relative detuning as a function of the excitation amplitude in the case of forced oscillations is given in Fig. 5b.

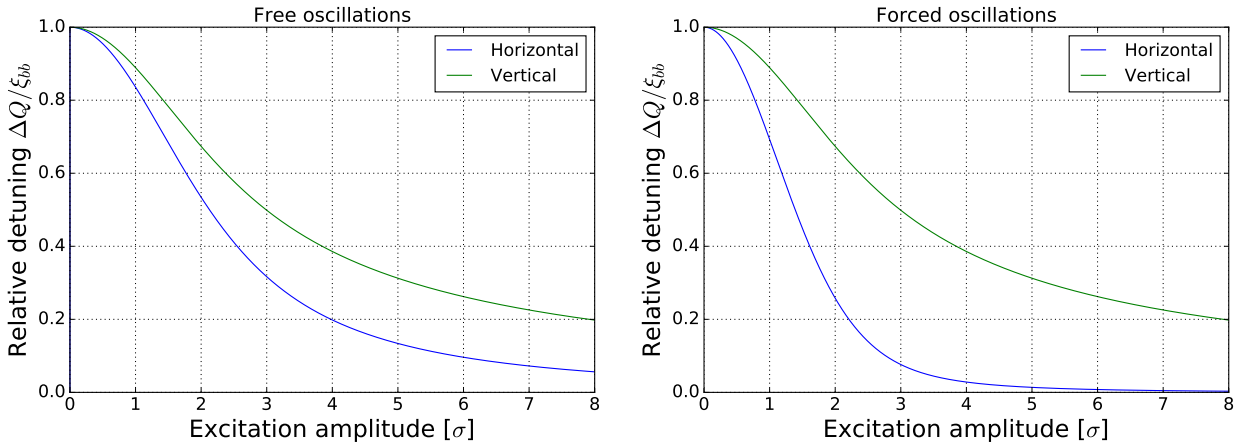

(a) Free oscillations on horizontal plane

(b) Forced oscillations on horizontal plane

Figure 5: Relative detuning versus the amplitude

Fig. 5 shows the relative beam-beam amplitude detuning for free and forced oscillations assuming an oscillation in the horizontal plane (Eqs. 6 to 9). The four curves have the same initial and asymptotic values as expected. Concerning the excited plane (horizontal), at small amplitudes, forced oscillations detune twice faster than the free oscillations. On the non-excited plane (vertical), the detuning is the same for both free and forced oscillations.

4 Beam-beam induced β-beating simulations

The analytical formulas presented in the previous section are a powerful tool to quickly evaluate the detuning with amplitude in the presence of beam-beam without simulations. However, as explained before, they are applicable in a weak-strong regime. In order to understand its limitations, the COMBI code is used for benchmark. Although mainly used for self-consistent simulations where the two beams are updated after each interaction, COMBI allows as well single particle tracking in a weak strong regime. The free oscillations are realized by tracking particles with different initial transverse amplitudes. In the case of forced oscillations, an AC dipole-like element was made available in the action list (action 7, sub-action 2).

4.1 Single particle

In order to validate the formulas in Section 3, the COMBI simulations are set in a weak-strong regime where a single particle is tracked through a beam-beam lens. In Fig. 6, the amplitude detuning simulations (dashed lines) versus initial (free) or excitation (forced) amplitude are compared with Eqs. 6 and 8 for free and forced oscillations respectively in the horizontal plane.

The forced excitation amplitude is computed from the Fourier amplitude of the spectral line (at the forced tune) during the excitation plateau and then normalized to the RMS beam 2 size to only consider the motion induced by action 7.

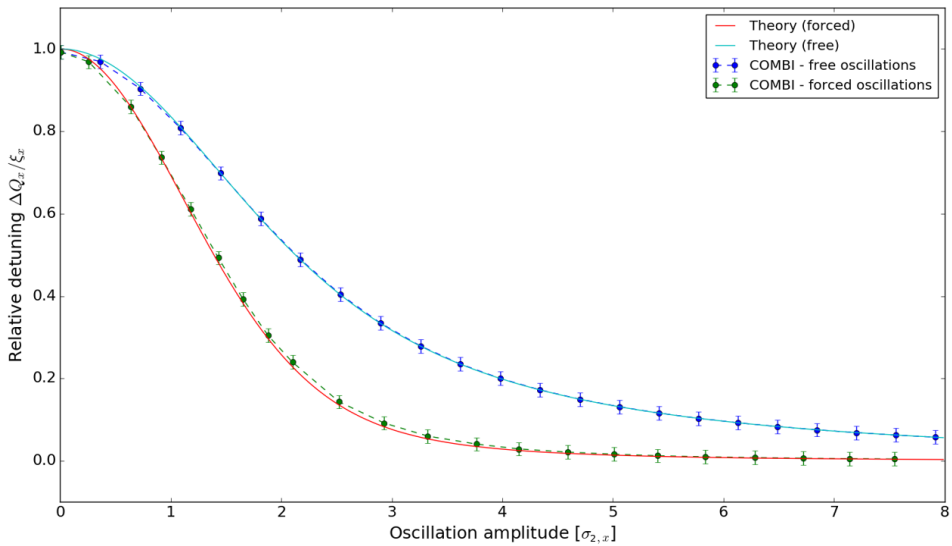

Figure 6: Simulated relative amplitude detuning versus free (dark blue) and forced (green) oscillation amplitude from single particle tracking simulations. Eqs 6 (light blue) and 8 (red) are also shown representing the analytical expressions expected for free and forced oscillations.

The agreement between the analytical expressions and the single particle tracking sim-

ulations from COMBI is extremely good probing their validity in weak-strong regimes.

4.2 Multi-particles

More realistic simulations with two equal bunches undergoing self-consistent interaction are now set to compare with the analytical estimations. The parameters used in the simulations are :

- One head-on interaction with $\beta^* = 1$ m
- LHC nominal collision tunes $(Q_x, Q_y, Q_s) = (64.31, 59.32, 0.005)$ and circumference (26.658 km)
- One bunch per beam at injection energy (450 GeV)
- 10^6 turns
- 10^5 macroparticles per bunch
- Forced oscillations in beam 1 on the horizontal plane at $Q_{driven} = 0.292$
- AC dipole ramp up 2000 turns

Multi-particle simulations (with bunches) are different from single particle (Sec. 4.1) in the sense that a bunch is constituted of particles with a given distribution of amplitudes. This means that the strength of the kick received by each one of them at the IP will be dependent on its amplitude (Sec. 2.1). Thus, we expect the incoherent detuning of the bunch particles to correspond to a spread that spans the interval 0 (very large amplitude particle) to ξ_{bb} (zero amplitude). The use of Eqs. 8 and 9 are then limited in this case due to the finite oscillation amplitude of the individual particles within the bunch. Fig. 7 illustrates the detuning of particles oscillating with different unperturbed oscillation amplitudes as a function of the forced oscillation amplitude.

Particles with a larger unperturbed oscillation amplitude feature a smaller tune shift versus the excitation amplitude as shown in Fig. 7 (red line, 6 σ particle). Particles with a non-zero unperturbed oscillation amplitude cross the analytical formula given by Eq. 8 (black curve), derived for particles with no unperturbed oscillation amplitude, between 2 σ and 3 σ. Thus, the analytical formula should represent the upper boundary of the incoherent spectrum below 2 σ and the lower boundary above 3 σ for forced oscillations. This phenomenon can be understood from the shape of the derivative of the beam-beam force (Fig. 3) that changes sign at about 1.6 σ. In the non-excited plane, we do not expect the same effect and the analytical formula (Eq. 9) should match the upper boundary of the incoherent spectrum.

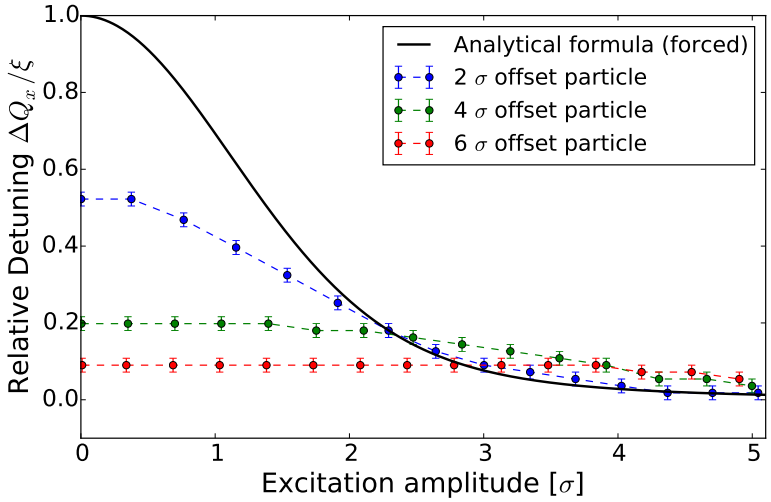

Figure 7: Simulated relative amplitude detuning versus forced oscillation amplitude for particles with increasing free oscillation amplitudes: 2 σ, 4 σ and 6 σ. Equation 8 is also shown representing the 0 σ particle.

Once the expected differences between multi-particle simulations and analytical estimations are set, other parameters are evaluated. Next, the damper effect, the impact of the intensity (number of protons per bunch) and emittance ratio between both beams are addressed. Table 2 summarizes the different cases simulated : impact of the ADT, intensity ratio and emittance ratio. Note that the beam-beam parameter from beam 2 was kept constant for the following simulations

Figures	ADT	$I_1[10^{11}$ ppb$]/I_2[10^{11}$ ppb$]$	$\varepsilon_{n,1}[\mu$m$]/\varepsilon_{n,2}[\mu$m$]$
8a & 8c	**off**	1/1	2/2
8b & 8d	**on**	1/1	2/2
9a & 9c	off	**0.7/1**	2/2
9b & 9d	off	**0.1/1**	2/2
10a & 10c	on	0.5/1	**1/2**
10b & 10d	on	0.5/1	**4/2**

Table 2: Overview of the simulation parameters. The differences between pairs of simulations are highlighted in bold.

4.2.1 Impact of the transverse feedback

We now study the impact of the transverse damper on beam 2 since we would like to get closer to the analytical derivation where the probe beam is almost a single particle with a small unperturbed oscillation amplitude.

Figure 8 shows beam 1 horizontal (top) and vertical (bottom) spectrograms as a function of the excitation amplitude without and with transverse feedback (damping time 1 turn) on beam 2 (left and right column respectively). The rest of the simulation parameters

remain the same. The black curve corresponds to the beam-beam amplitude detuning on the related plane for forced oscillations (Eq. 8 and 9 on the horizontal and vertical plane respectively).

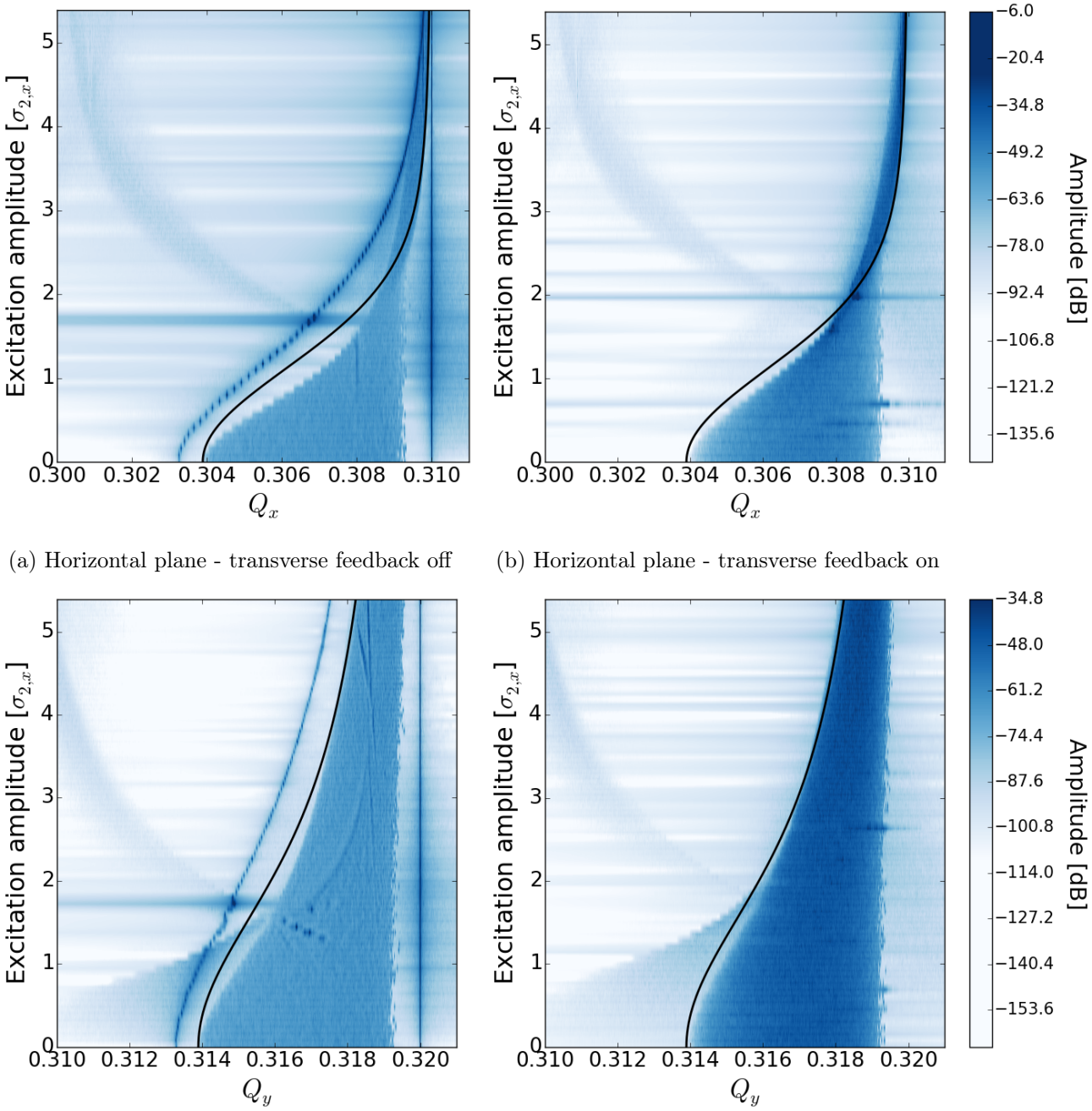

(a) Horizontal plane - transverse feedback off

(b) Horizontal plane - transverse feedback on

(c) Vertical plane - transverse feedback off

(d) Vertical plane - transverse feedback on

Figure 8: Simulated beam 1 spectrograms versus horizontal amplitude of forced oscillations with (left) and without (right) transverse feedback on beam 2

Coherent beam-beam modes

When the feedback system is turned off as in Fig. 8a and 8c, none of the beams coherent oscillations are damped and coherent beam-beam modes between the beams are visible. The σ-modes are located at the unperturbed tunes $Q_0 = (0.31,\ 0.32)$ as expected and are discrete modes distinct from the incoherent spectrum. The π-modes also appear as distinct discrete modes at lower frequencies, on the other side of the incoherent spread. Being discrete modes outside the incoherent spread can lead to beam instabilities since such modes cannot be stabilized by Landau damping [33]. In these conditions, the coherent beam-beam effects could drive the π-mode to large amplitudes which may lead to the loss of the beam.

The frequency of the π-mode when no forced oscillations are applied is approximately $Q_\pi = (0.3032,\ 0.3132)$. Given that $\xi_{bb} = 0.0061$, the Yokoya factor is close to 1.1 as expected. The π-mode frequency changes over the excitation amplitude of the forced oscillations and converges to the unperturbed tune. The presence of a transverse feedback on beam 2 avoids the formation of coherent beam-beam modes as shown in Fig. 8b and 8d. The expected spectrum changes and this represents better the measurements conditions of the LHC where an ADT is operationally used to suppress coherent oscillations.

Incoherent spectrum

The incoherent spread in the spectrum with no forced oscillation (i.e. only beam-beam interaction) in Fig. 8 spans the interval between the unperturbed tunes Q_0 and $Q_0 - \xi_{bb}$ corresponding to the limit value of the black curve for small amplitudes as expected.

On the horizontal plane, the influence of the transverse feedback on the upper boundary of the incoherent spectrum (below 2 σ) is visible when comparing Fig. 8a and 8b. Indeed, in the case with a transverse feedback on beam 2 (Fig. 8b), the upper boundary of the incoherent spectrum is closer to the analytical expression below 2 σ. Above 3 σ, the lower boundary of the incoherent spectrum fits the analytical expression from a smaller excitation amplitude (2.7 σ vs 3.2 σ).

In the vertical plane (bottom Fig. 8), the presence of the transverse feedback (Fig. 8d) makes the upper boundary of the incoherent spread closer to the analytical expression compared to the case without transverse feedback (Fig. 8c). The difference is specially visible until $\sim 3\ \sigma$.

Therefore, the deviation between the tune of the zero amplitude particles and Eqs. 8 and 9 decreases when including a transverse feedback on beam 2. Indeed, when there is no transverse feedback, the beam-beam force is modified by the presence of low amplitude coherent oscillations of the two beams and the analytical derivations do not model these effects accurately. The presence of a transverse feedback allows us to be closer to a weak-strong regime since beam 2 is unable to excite the oscillating beam (beam 1) in return.

Curved resonance

A bent line originating in the top left corner crosses the spectrogram in all the spectrograms from Fig. 8. This line matches with a resonance excited by the AC dipole that has a dependence on the π-mode of the form : $C - 2Q_\pi$, where C is a constant. Further investigations are needed to address the origin of this line. This resonance appears in all the plots where forced oscillations were used regardless the intensity or emittance ratio between both beams.

Horizontal line $\sim$ 1.8 σ

In Fig. 8a and 8c, the spectrum for an excitation amplitude around 1.8 σ_x is dominant. Additional simulations with a different driven frequency of the AC dipole were performed and showed that this line appeared for a different Q_π. It means that, at this given excitation frequency ($Q_{driven} = 0.292$), the forced oscillations excite the π-mode, which is a dangerous configuration since it could lead to strong beam instabilities.

4.2.2 Impact of intensity unbalance

We now study the influence of the beams intensity ratio. The aim here is to get closer to the analytical derivation where the probe beam is almost a single particle with a small unperturbed oscillation amplitude.

Figure 9 shows beam 1 horizontal (top) and vertical (bottom) spectrograms as a function of the excitation amplitude for intensity ratio of 0.7 and 0.1 between both beams (left and right column respectively). No transverse feedback was included in these simulations and the other simulation parameters remain the same. The black curve corresponds to the beam-beam amplitude detuning on the related plane for forced oscillations (Eq. 8 and 9 on the horizontal and vertical plane respectively).

Coherent beam-beam modes

When the intensity ratio is 0.7 (Fig. 9a and 9c), the spectrograms are altered with respect to the one where both beams are symmetric (Fig. 8a). Since we do not have transverse feedback on beam 2, the beam-beam coherent beam-beam modes from Fig. 8a and 8c are still present. However, the π-mode gets closer to the upper boundary defined by the incoherent spectrum and even begins to merge with the incoherent spectrum. As this intensity ratio decreases, additional simulations showed that the π-mode merges progressively with the continuum incoherent spread and becomes less and less strong till it becomes not visible. The intensity scan was consistent with previous studies of coherent beam-beam modes [27] showing that for an intensity ratio below 0.6, the π-mode merges into the incoherent spectrum and is Landau damped. For example, for an intensity ratio of 0.1 as shown by Fig. 9b and 9d, the π-mode has completely merged with the incoherent spread and it is not distinguishable anymore even though there is no transverse feedback.

The σ-mode in Fig. 9 is still present and is not affected by a change in intensity ratio. It corresponds to the very thin line at the unperturbed tunes $Q_0 = (0.31,\ 0.32)$.

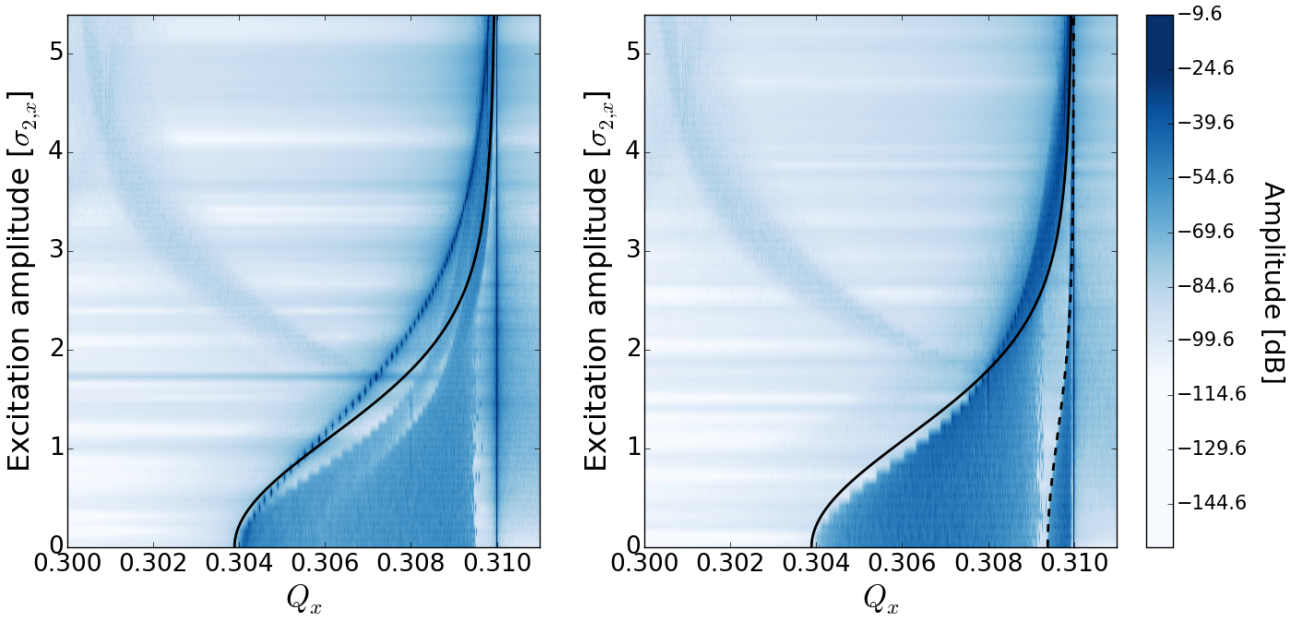

(a) Horizontal plane - I ratio 7/10

(b) Horizontal plane - I ratio 1/10

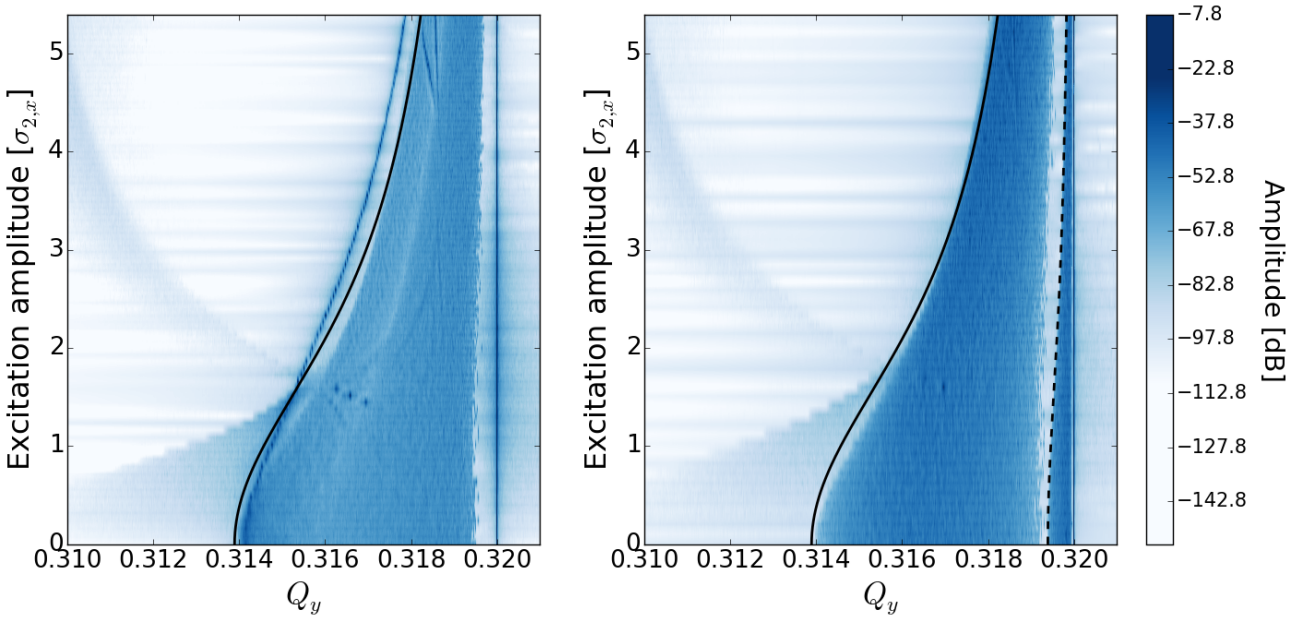

(c) Vertical plane - I ratio 7/10

(d) Vertical plane - I ratio 1/10

Figure 9: Simulated beam 1 spectrograms versus horizontal amplitude of forced oscillations for intensity ratio 7/10 (left) and 1/10 (right) between beam 1 and 2

In Fig. 9b and 9d, the wider signal close to the unperturbed tunes does not represent the σ-mode from beam 1. The dotted line is computed the same way the solid line is but using the beam-beam parameter felt by beam 2, i.e. with beam 1 parameters. The agreement between this dotted line and the incoherent spectrum reveals that this wide signal is originating from beam 2 and that it corresponds to the incoherent spread due

to the beam-beam amplitude detuning of beam 2. The absence of transverse feedback on beam 2 made it possible to oscillate like beam 1 (forced oscillation) and since beam 2 has a factor 10 greater intensity, it appears on beam 1 spectrogram.

Incoherent spectrum

As beam 1 intensity decreases with respect to beam 2, the boundaries of the incoherent spectrum are described better by the analytical expression as expected. Indeed, when the ration I_1/I_2 gets smaller, the influence that beam 1 has over beam 2 from the beam-beam point of view becomes less and less important such that we are getting closer to a weak-strong regime where one of the beams does not affect the other at collision.

4.2.3 Impact of emittance unbalance

We now study the influence of the beams emittance unbalance on beam-beam. The aim here is to get closer to the analytical derivation where the probe beam is almost a single particle with a small unperturbed oscillation amplitude.

Figure 10 shows beam 1 horizontal and vertical (top and bottom respectively) spectrograms as a function of the excitation amplitude for emittance ratio of 0.5 (left) and 2 (right) between beam 1 and 2. The other simulation parameters remain the same. A transverse feedback (20 turns) was included in these simulations, therefore, the coherent beam-beam modes will be damped. The black curve corresponds to the beam-beam amplitude detuning for forced oscillations (Eqs. 8 and 9 respectively).

Incoherent spectrum

The comparison of the horizontal spectrograms (Fig. 10 top) with the two different emittance ratio shows that the deviation between the upper boundary of the incoherent spectrum below 2 σ and the analytical expression (solid line) is smaller in the case where beam 1 emittance is smaller than beam 2 emittance. On the vertical plane (Fig. 10 bottom), the upper boundary of the incoherent spectrum is also slightly closer the analytical expression when one has an emittance ratio smaller than 1. As beam 1 emittance decreases with respect to beam 2, we get closer to a weak-strong regime where the single particle has an emittance almost zero. These observations are consistent with the fact that we are approaching a weak-strong regime where beam 1 influence over beam 2 is smaller.

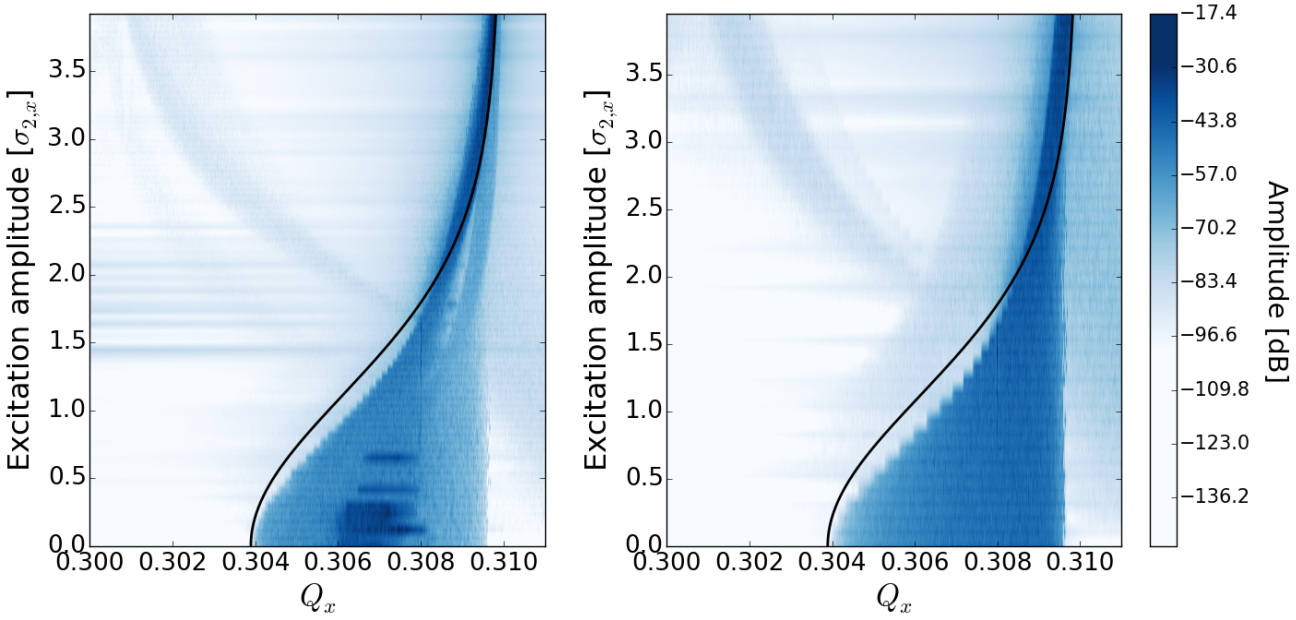

(a) Horizontal plane - ε_n ratio 1/2

(b) Horizontal plane - ε_n ratio 4/2

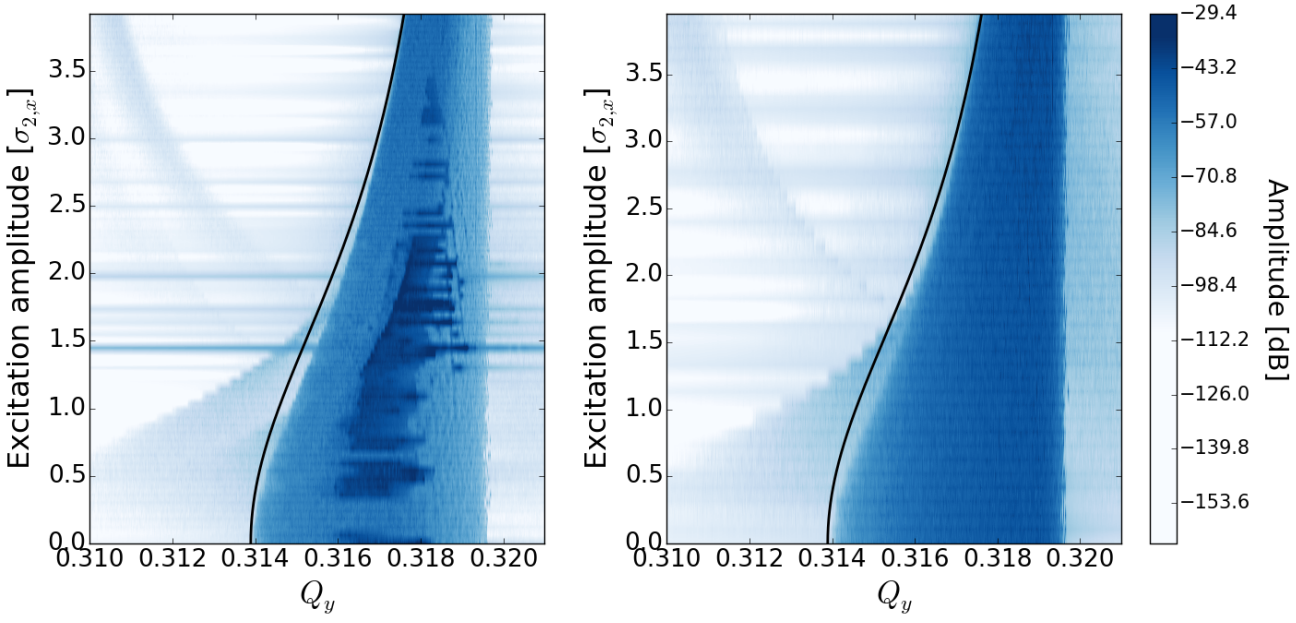

(c) Vertical plane - ε_n ratio 1/2

(d) Vertical plane - ε_n ratio 4/2

Figure 10: Simulated beam 1 spectrograms versus horizontal amplitude of forced oscillations for emittance ratio 1/2 (left) and 4/2 (right) between beam 1 and 2

4.2.4 Impact of collisions with offset

We now study the influence of a static horizontal offset between the beams at the IP (without forced oscillations).

Simulated spectrograms are presented in Fig. 11. Both beams are here symmetric (same intensities and emittances) and a transverse feedback (20 turns) is activated on beam 2. The dotted black lines correspond to the tune of the zero amplitude particles.

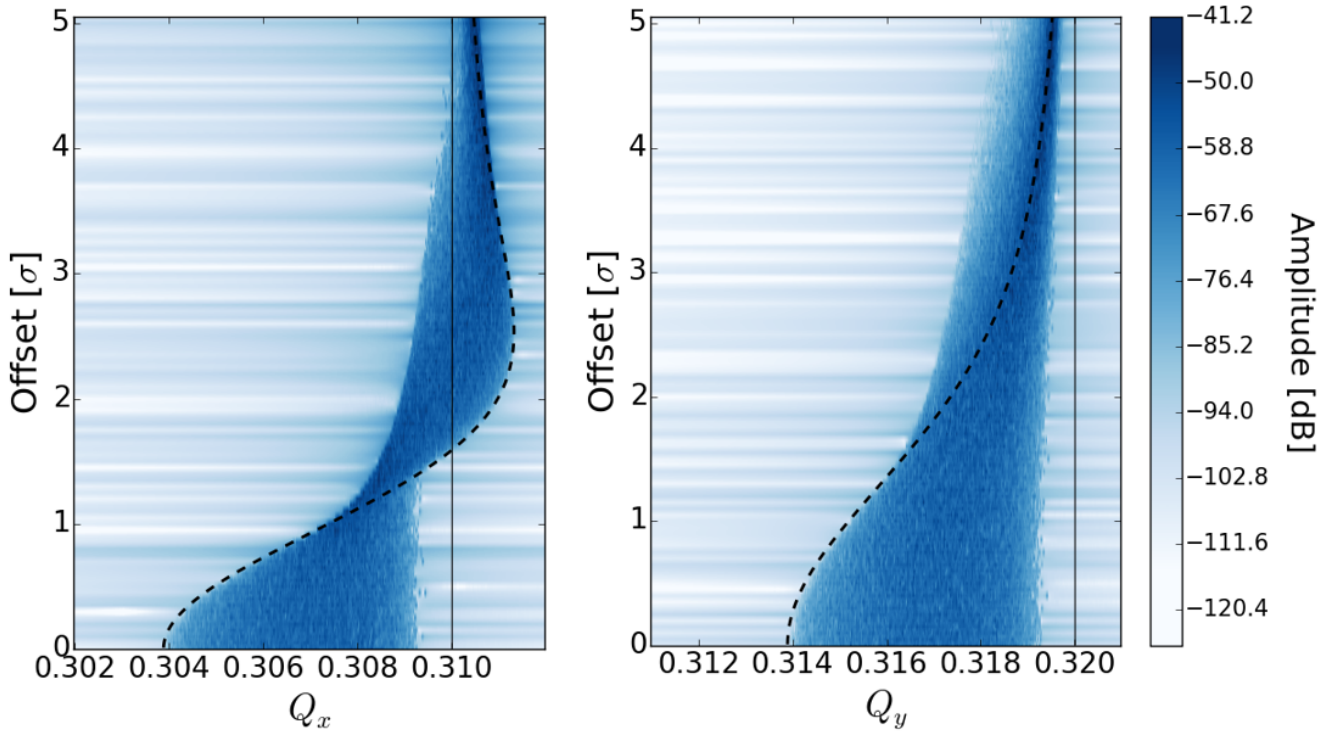

(a) Horizontal beam 1 spectrum

(b) Vertical beam 1 spectrum

Figure 11: Simulated frequency beam 1 spectrograms versus horizontal offset between both beams at the IP

Since we are increasing the static offset horizontally, the zero amplitude particle detuning in the horizontal spectrum (Fig. 11a) is related to the derivative of beam-beam force shown in Fig. 3. The upper boundary of the incoherent spread matches the analytical detuning below approximately 1.1 σ and the lower boundary for a greater offset as expected.

The offset introduced in the horizontal plane has a different influence on the vertical spectra (Fig. 11b). In this case, the detuning of the zero amplitude particle can be derived from the derivative of the force (Eq. 3) with respect to the vertical coordinate and an offset needs to be set in the horizontal plane. The zero amplitude particles correspond in this case to the upper boundary of the spectrum until $\sim 1.5\ \sigma$ and they converge then to the unperturbed vertical tune $Q_{0,y} = 0.32$.

5 Beam-beam induced β-beating measurements

5.1 Procedure

In the future HL-LHC and FCC-hh, the optics distortions induced by the beam-beam interactions will exceed tolerances (Table 1). For this reason, it is necessary to assess whether it is possible to measure the β-beating during collision and eventually correct it especially since previous attempts in other colliders failed [34]. A 8 hours Machine Development study was dedicated to this topic between the 29th and the 30th of October 2016. In Fig. 12, an overview of the experiment is shown with two distinctive periods. Three bunches were injected in the first period of the MD in order to find collisions at IP1, to test the reproducibility of the separation bumps and to setup the ADT [16] and AC dipole [15] as exciters. The second period is made out of five injections, where one pilot bunch was injected with the damper set up for beam 1 and two nominal bunches were injected in beam 2.

The MD was performed at injection energy (450 GeV) since the head-on interaction is energy independent and a higher beam-beam parameter ξ_{bb} can be reached due to the geometric emittance reduction. The separation bump was collapsed in IP1 and the transverse damper was turned off on beam 1. Through the five injections constituting the second part of the MD, AC dipole or ADT excitations with different excitation frequencies and amplitudes were applied on beam 1 while a transverse feedback was activated on the strong beam with a damping time of 50 turns. The excitation amplitudes are always given in units of the RMS beam size σ at the IP. The length of the excitations was in the order of 6600 turns for the AC-dipole and 29000 for the ADT. In order to ensure the adiabaticity of the AC dipole excitation, the amplitude was ramped up in 1100 turns [24].

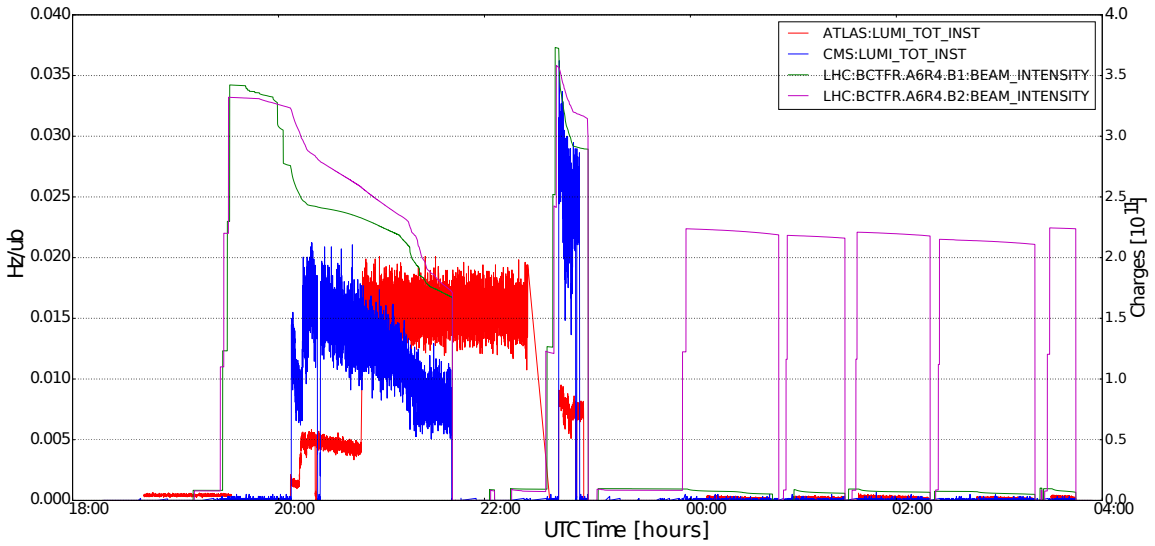

Figure 12: Overview of the MD 979 between 2016-10-29 18:00:00 and 2016-10-30 04:00:00 (UTC time). The set-up period, until around 23:00:00, is shown together with the five fills where the excitations were carried out.

5.2 Beams parameters

In order to eliminate uncertainties during the measurements and simplify the scenario, it was chosen to collide in a weak-strong regime. To achieve this, one order of magnitude difference on intensity between the beams was requested from the injectors. In Fig. 29 (appendix A), the intensities of beam 1 (left), weak beam, and beam 2 (right) are plotted as a function of time.

The horizontal and vertical emittances of beam 1 and 2 measured by the Beam Synchrotron Radiation Telescope (BSRT) system [35] are shown in Fig. 30 (appendix B, left and right respectively). To enhance the beam-beam parameter, small beams were requested (0.5-1.0 μm). However, the BSRT system is calibrated for normal operation condition which means that for $\varepsilon_n < 1.5$ μm, an uncertainty up to 30% [36] on the values measured is expected. Furthermore, the effect of the β-beating due to the beam-beam collision at the location of the BSRT has to be evaluated since it could increase the uncertainty on the emittance of another 8% for this case (collision at one IP). Besides the growth rates expected, a blow up can be observed at the end of the 3$^{\text{rd}}$ and 4$^{\text{th}}$ fill in both beams caused by the too large excitation amplitudes used. The first beam also seems to have blown up during the first fill. Investigations are still in progress in order to determine the cause of it.

The horizontal and vertical beam tunes were the collision ones (0.31, 0.32), the full crossing angle at IP1 and IP5 was 340 μrad and β^*=11 m.

5.3 Beam spectra

An example of the beam spectra measured by the Base-Band Tune (BBQ) system [37] for beam 1 is shown in Fig. 13. The red curve represents the beam frequency spectrum during the ADT excitation and the blue one represents the beam spectrum just before with the beams already in collision. Before the excitation (blue line), the beam-beam parameter, measured as the continuum incoherent spread starting at approximately 0.292 (Fig. 13 right), is $\xi_{bb} = 0.018$ which is smaller than what was initially computed with beams parameters from Sec. 5.2. In other words, the derived value of the normalized emittance from the BBQ spectrograms is larger than the one measured by the BSRT system which points again towards larger emittances. The comparison of the beam-beam spread before (blue) and during the excitation (red) for different amplitude excitation shows that for a small amplitude case (Fig. 13 left, 0.55 σ_x) the spread during excitation Ξ_{bb} is larger than for a larger excitation amplitude (Fig. 13 right, 1.19 σ_x). In the limit of very large excitation, the incoherent spectrum would reduce to a single peak close to the collision tune.

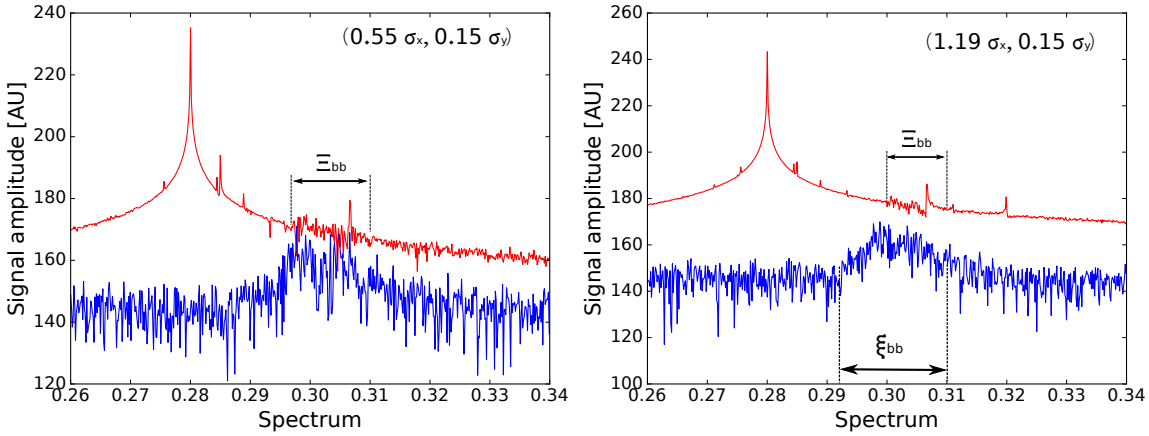

Figure 13: Horizontal spectra of beam 1 for different ADT excitation amplitudes. The vertical excitation amplitude is always $0.15\sigma_y$ and the horizontal one is $0.55\sigma_x$ and $1.19\sigma_x$ for the left and right plot respectively. The blue curve corresponds to the spectrum of the beam just before the ADT excitation whereas the red one to the spectrum during the excitation. The horizontal and vertical ADT excitation frequencies were (0.28, 0.285).

The excitation in the vertical plane (0.15 σ_y at 0.285) can be observed on the horizontal spectra from Fig. 13 since both planes are coupled through the beam-beam force. As the horizontal excitation amplitude increases, the signal from the vertical excitation merges gradually with the horizontal excitation peak located at 0.28.

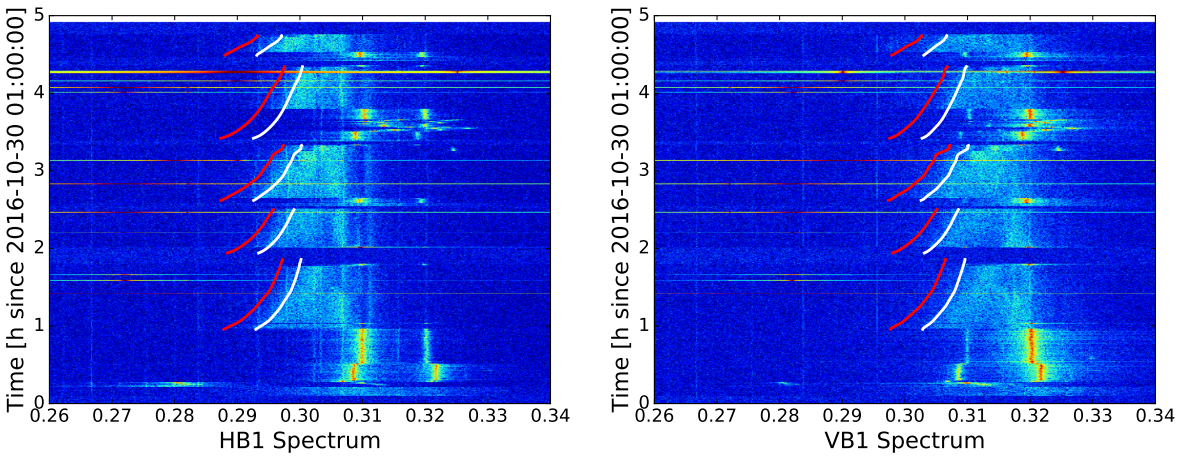

(a) Horizontal beam 1 spectrum from BBQ

(b) Vertical beam 1 spectrum from BBQ

Figure 14: BBQ Spectrograms of the MD for both planes where the red and green curve represent the tune of the zero amplitude particles after beam-beam collision for no correction factor and a 20% larger beam 2 emittance respectively

The complete beam 1 spectrograms, for both horizontal and vertical planes, during the five fills of the second period of the MD measured by the BBQ system are shown in Fig. 14. The two curves on the spectrogram (red and white) indicate the beam-beam tune shift of

the zero σ amplitude particles, i.e. $Q_0 - \xi_{bb}$. The red one is calculated using the beam 2 parameters presented in Section 5.2 without any correction factor for the emittance while the white one takes into account a 20% larger emittance of beam 2 in both planes leading to a smaller beam-beam parameter (between 0.0185 and 0.011). The 20% correction factor on the emittances provides better agreement with the BBQ observations: the largest particles tune shift matches a 15% to 20% larger emittance.

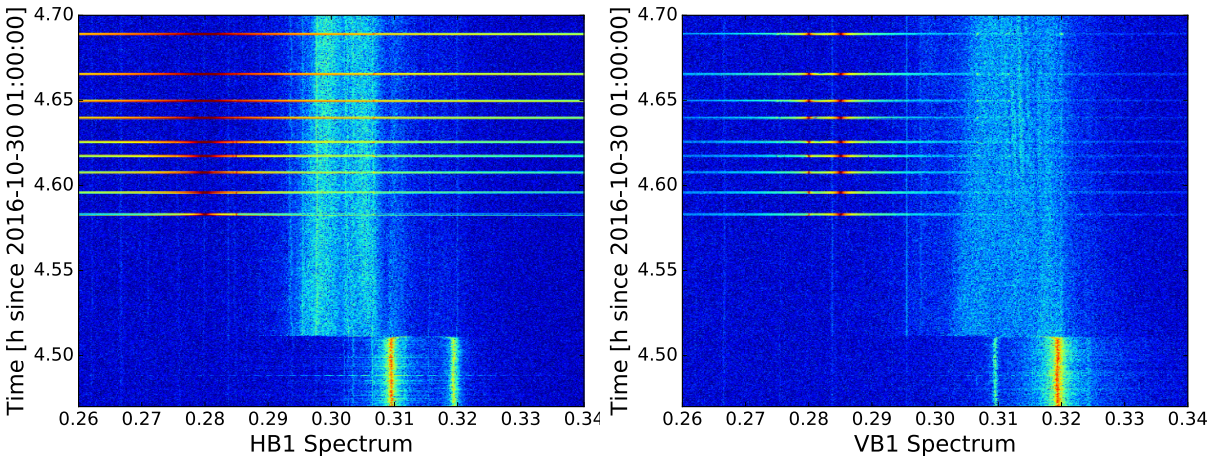

(a) Horizontal ADT excitations (0.28) (b) Vertical ADT excitations (0.285)

Figure 15: Zooms on BBQ from Fig. 14a and 14b respectively in 5$^{\text{th}}$ fill

In Fig. 15, zooms of the 5th fill in Fig. 14 with ADT excitations are shown. These excitations contain the spectrum shown in Fig. 13. The horizontal and vertical tunes of the beam 1 are clearly seen before the start of the collision. From about 4.52 on the y-axis, both beams enter in collision leading to the incoherent spread. The ADT excitations were kept constant in the vertical plane (0.15 σ_y) and increased in the horizontal plane (from 0.27 σ_x to 1.3 σ_x). The horizontal and vertical excitations made with the ADT device (0.28, 0.285) are visible on the spectrograms of both planes with stronger signal for the excitation in the related plane. Some vertical lines (e.g. at $\sim$ 0.295) can also be noticed on Fig. 15a and 15b. They do not correspond to resonances since they are present before and after collision, they actually are artifacts from the BBQ system.

5.4 Natural tune

During this MD, forced oscillations driven by the AC dipole and ADT are used to reconstruct the β-function along the machine using the N-BPM method [38]. However due to the fact that forced oscillations differ from the free oscillations, a correction is required based on the distance from the natural and driven frequencies [39]. When there is no collision, both of these frequencies are well defined (the natural tunes corresponds to the unperturbed tunes of the beams). However, in collision, the tunes are not well defined anymore given the incoherent spread of the beam due to beam-beam effect. This is why

the possibility of finding a tune that would allow the computation of the β-function in collision (i.e. natural tune) is explored in what follows.

Three different approaches based on Beam Position Monitors (BPM) readings were explored to deduce the best natural coherent tune at collision: (i) direct observation of the natural tune in the beam 1 spectrum, (ii) phase propagation in IR4 using the segment-by-segment analysis [40, 41] and (iii) minimization of the RMS β-beating on both sides of the AC Dipole/ADT location. Once the best natural tune is found, the β-function due to beam-beam can be reconstructed and the β-beating computed.

An example of beam 1 spectrum for the strongest AC-dipole excitation (end of 1st fill) is shown in Fig. 16. The AC-dipole excitation, at frequency (0.268, 0.278), is the largest peak on both planes as expected. The excitation from the opposite plane is also present on both spectrums due to the coupling between the horizontal and vertical plane. On the horizontal plane (Fig. 16a), an octupolar secondary line resonance of the fourth order ($-Q_x^{AC} + 2Q_y^{AC} = 0.288$) is observable. On the vertical plane (Fig. 16b), a dodecapolar secondary line of the sixth order ($-2Q_x^{AC} + 3Q_y^{AC} = 0.298$) is present. Only even orders are generated by head-on collision due to the symmetric potential as expected [42]. It is the first time that resonances from beam-beam interaction with such high orders are observed. The last distinguishable peaks that are present might correspond to the beam natural tune appearing at the frequencies (0.307, 0.317), which is close to the initial tunes and consistent with large amplitude kicks. However, there is not always a clear signal of the natural tune so this approach could not be used for other AC-dipole or ADT excitation measurements.

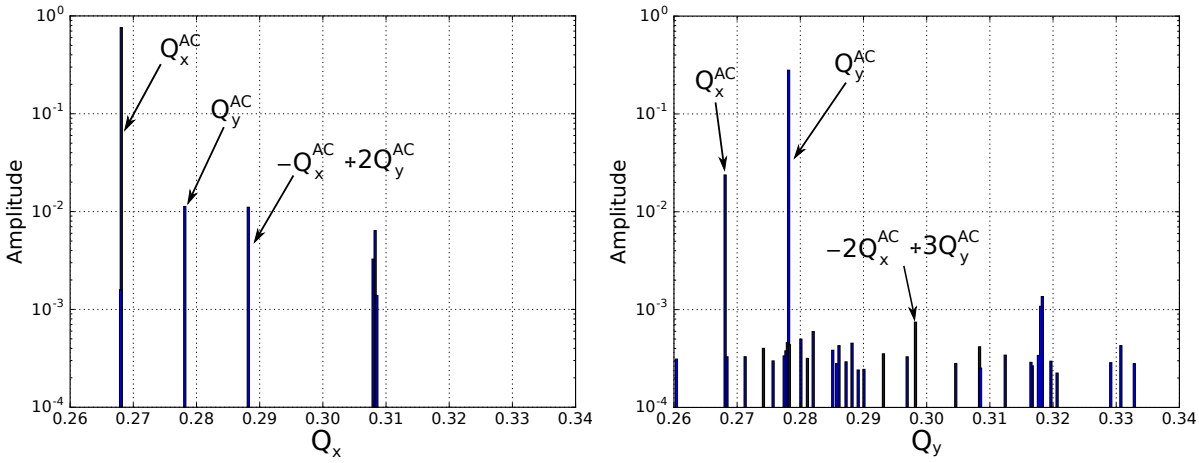

(a) Horizontal spectrum with $1.8\sigma_x$ excitation amplitude

(b) Vertical spectrum with $1.84\sigma_y$ excitation amplitude

Figure 16: Beam 1 spectra of the strongest AC-dipole excitation ($Q_{driven} = (0.268,\ 278)$) of the 1st fill at the BPM.6R2

The phase advance method consists in the computation of the phase advance beating originating at the location of the excitation device (IR4) using the BPMs data. The phase

advance beating corresponds to the difference in phase advance between the computed phase advance from the model and the one deduced from the BPMs measurements. The phase advance of the betatron oscillation between the BPMs is computed using the BPMs turn-by-turn data [40]. This method is based on minimizing this beating by scanning the natural tune parameter. The latter is applied to the IR4 segment which is treated as an independent transfer line, meaning that the measured optics are used as initial conditions for the simulations and that the machine errors occurring in this segment are neglected in the phase propagation. The scans in natural tunes provide the same results indicating the best natural tunes were (0.31, 0.32). Further analysis about the simulations and limitations of the model are still in progress.

The RMS method is based on the fact that the largest β-beating source for forced oscillations in IP4 should be the AC dipole/ADT itself. Thus, the best guess of the natural tune should minimize the difference of the RMS β-beating due to beam-beam between both sides of IP4. This method provides coherent values of the natural tunes for every excitation in the sense that the stronger is the excitation, the closer to the initial tunes is the natural tune. Horizontal and vertical scan of the natural tune with two different AC-dipole excitations of the 1st fill are shown in Fig. 17. In the case of the strongest AC-dipole excitation (1.8 σ_x and 1.84 σ_y on the x-y plane), the natural tunes provided by this method (green curves in Fig. 17a and 17b) are (0.31, 0.3163), which are close to the ones from the spectra analysis from the same excitation (Fig. 16) : (0.307, 0.317). The natural tune at collision provided by the above methods for the strongest AC dipole excitation was assumed to be $(0.3085 \pm 0.0015,\ 0.3165 \pm 0.0010)$.

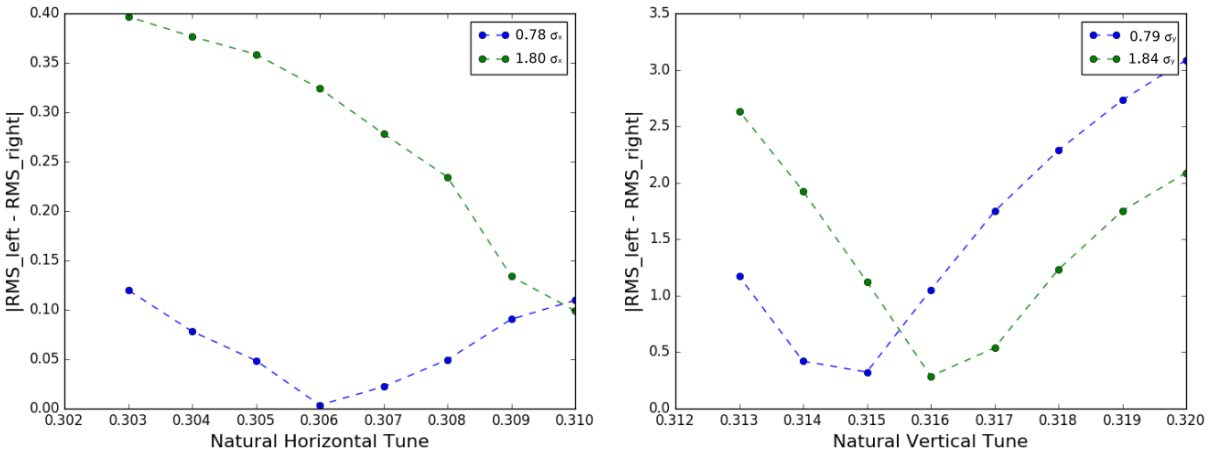

(a) Horizontal plane

(b) Vertical plane

Figure 17: Scan of the natural tune for horizontal and vertical plane. Both lines are for AC-dipole excitations from the 1st fill with different excitation amplitudes.

Multi-particle simulations were made mimicking the MD parameters using COMBI. A scan in forced oscillation amplitude was made as in Sec. 4.2 as shown in Fig. 18. Both secondary lines found on beam 1 spectrums (Fig. 16) are present on the spectrograms

computed with COMBI. The spread close to the unperturbed tunes (0.31, 0.32) correspond to beam 2 spread since the beam-beam parameter acting on beam 2, i.e. computed with beam 1 parameters, is more than 10 times smaller than the other one (similar observation as in Fig. 9b and 9d). The natural tunes at collision from above are located in the incoherent spread of the beam.

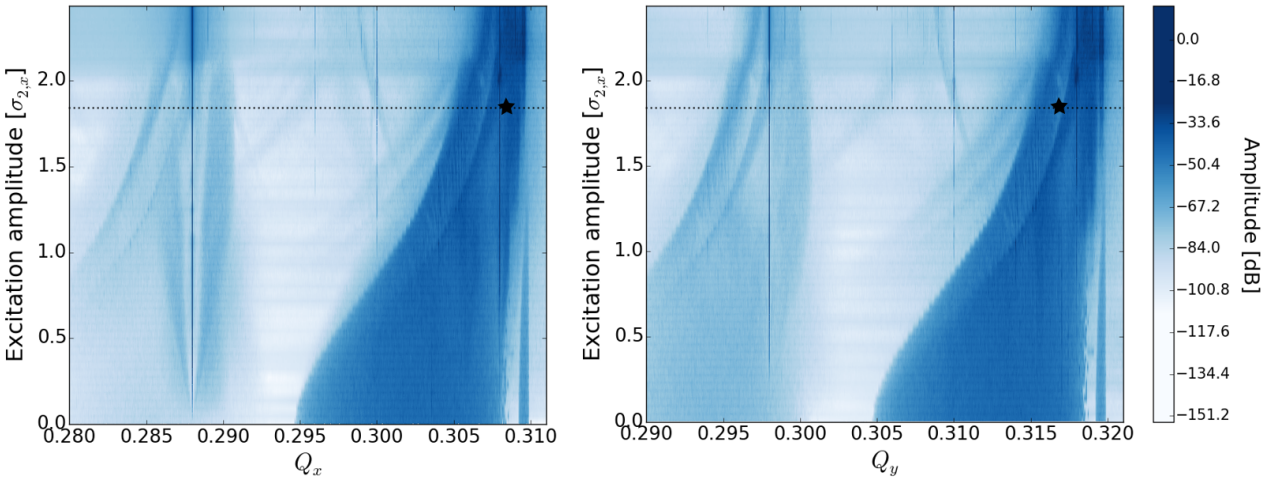

(a) Horizontal beam 1 spectrum

(b) Vertical beam 1 spectrum

Figure 18: Simulated frequency spectrograms for the horizontal (left) and vertical (right) planes versus amplitude of forced oscillations in the weakly interacting beam

5.5 β-beating due to beam-beam

We only consider in this section the strongest AC dipole mentioned above. The unperturbed β-function (β_0) was computed using the BPMs data, the driven tunes of the AC dipole $Q_{AC} = (0.268, 0.278)$ and the collision tunes $Q = (0.31, 0.32)$ with a measurement without beam-beam at the beginning of the first fill.

At collision, the natural tunes assumed for the β-function calculation are the ones from the previous sub-section. Beam 1 and beam 2 intensities are $6.2{\cdot}10^9$ ppb and $1.1{\cdot}10^11$ ppb and their emittances (1.1 μm, 1.3 μm) and (1.0 μm, 0.9 μm), respectively. The β-beating due to the beam-beam collision at IP1 (s=20 km) for the strongest AC dipole excitation (1.8 σ_x, 1.84 σ_y) is shown in Fig. 19.

The β-beating due to beam-beam collision remains below 10% and its maximum is about 7% in both planes. For the vertical plane, an important unexpected contribution from IP5 (s=6.6 km) is found. Further investigations are needed to fully understand its cause, as the beams were kept separated at that location.

Since the β-beating is amplitude dependent [43], the previous measurements must be compared to simulations including forced oscillations. In this purpose, MAD-X simulations with the beam parameters mentioned above predict a 1.8 σ particle β-beating as shown in Fig. 20. Two different scenarios are simulated : using the measured emittance from the

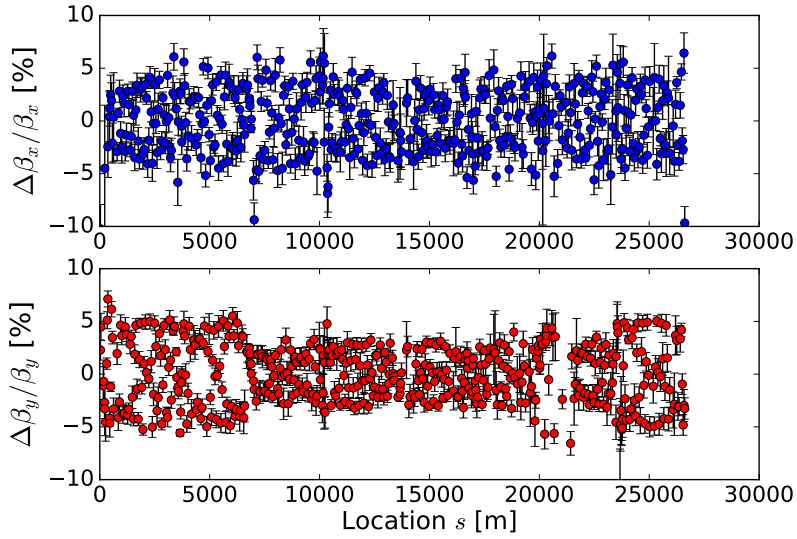

Figure 19: Measured β-beating for 1.8 σ_x and 1.84 σ_y amplitude particle due to beam-beam interaction at IP1 along the machine computed from BPMs data. This case corresponds to the AC dipole excitation shown on Fig. 16 and to the green plot on Fig. 17. The longitudinal coordinate starts at IP3.

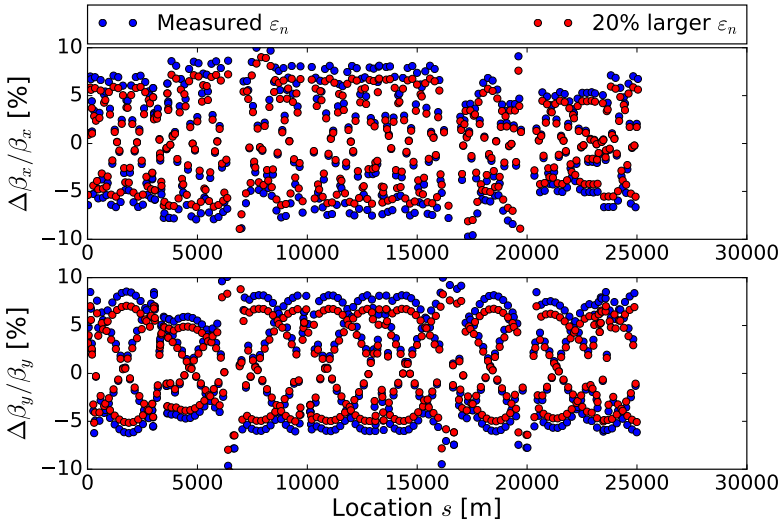

Figure 20: Simulation of β-beating in the LHC due to head-on beam-beam interaction at IP1 at injection energy for 1.8 σ amplitude particle. Blue points were computed based on the measured normalized transverse emittance from BSRT system and the red ones assuming a 20% larger emittance. The longitudinal coordinate starts at IP3.

BSRT system and with a 20% increase. The maximum β-beating is about 6% and 8% with and without the correction factor respectively. The comparison of the β-beating results from Fig. 19 with the expected one from simulations shows that simulations and measurements are of the same order of amplitude. The 20% correction factor to the emittance provides a smaller β-beating as expected that is more consistent with the measurements.

6 Beam-beam impact on luminosity production for the FCC-hh

In the previous sections, it was studied in detail the impact of the beam-beam interaction on the optics along the machine. In addition to the change of optics in strong-strong regime, both beams will interact modifying their distributions and diverging from an ideal Gaussian. The impact of the luminosity production has to be evaluated in those cases.

In order to derive the general expression of the luminosity, one has to take into account both beams distribution and integrate the overlap of density in space and time. The spatial coordinate defined by x, y and s correspond to the horizontal, vertical and longitudinal directions respectively. The temporal coordinate is defined by s_0, the distance of the two bunches to the central collision point. In the case of two different beams distributions ρ_1 and ρ_2, the luminosity can be written as [44]:

$$\mathcal{L} = N_1 N_2 f N_b K \iiiint_{-\infty}^{+\infty} \rho_1(x, y, s, s_0)\rho_2(x, y, s, s_0)\, dx\, dy\, ds\, ds_0, \tag{10}$$

where $K = \sqrt{(\vec{v_1} - \vec{v_2})^2 - (\vec{v_1} \times \vec{v_2})^2}/c$ is a kinematic factor. Assuming we have head-on collisions ($\vec{v_1} = -\vec{v_2}$) and the beams distributions to be uncorrelated in all planes, the luminosity expression can be factorized as follow :

$$\mathcal{L} = 2N_1 N_2 f N_b \int_{-\infty}^{+\infty} \rho_{1x}(x)\rho_{2x}(x)\, dx \int_{-\infty}^{+\infty} \rho_{1y}(y)\rho_{2y}(y)\, dy \iint_{-\infty}^{+\infty} \rho_{1s}(s-s_0)\rho_{2s}(s+s_0)\, ds\, ds_0. \tag{11}$$

In order to quantify the influence of the collision on the luminosity, particle distribution along the three spatial axis (x, y and s) were generated using COMBI simulations with the following parameters:

- One head-on interaction where $\beta^* = 1$ m
- FCC-hh tunes $(Q_x, Q_y, Q_s) = (111.31, 109.32, 0.00116)$, circumference (97749.14 m)
- One bunch per beam at top energy (50 TeV)
- Particle distribution generated after 10^5 turns
- $5 \cdot 10^6$ macroparticles per bunch

Five different ways of computing the luminosity are presented :

- Gaussian distribution and unperturbed beam size assumed, i.e. σ remains constant (Eq. 2)
- Gaussian distribution assumed and deduction of beam size $\sigma_{x,y}$ (from Eq. 2) using fit on COMBI output data
- Double Gaussian distribution assumed and deduction of luminosity using the related fit on COMBI output data
- No assumptions on the distribution and numerical integration using COMBI output data (Eq. 11)
- Gaussian distribution assumed (Eq. 2) and use of the dynamic β formula to compute new beam size $\sigma_{x,y}$ (Eq. 4)

6.1 Transverse feedback on

COMBI simulations were performed including a transverse feedback on both beams with a damping time of 20 turns. A scan of the luminosity over the beam-beam parameter ξ_{bb} is presented in Fig. 21.

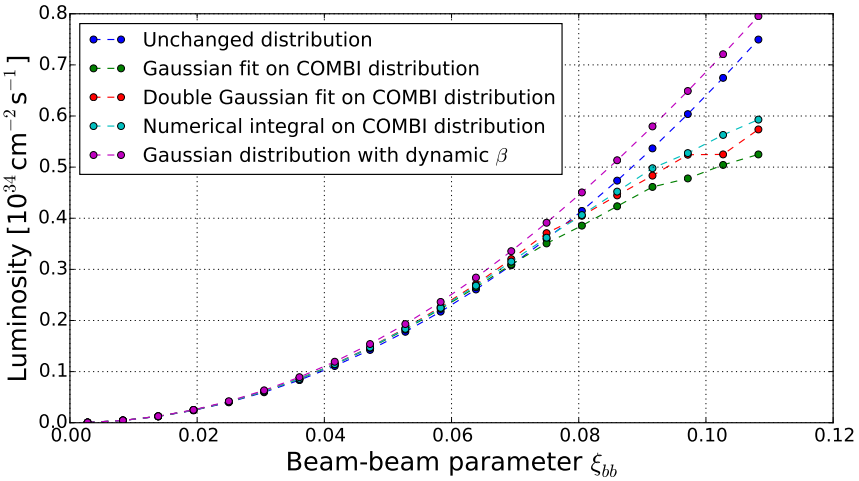

Figure 21: Luminosity as a function of the beam-beam parameter ξ_{bb}. The blue, green, red, light blut, purple curves correspond to the luminosity computed assuming a Gaussian particle distribution (Eq. 11) with the input RMS beam sizes, with RMS beam size derived using a Gaussian fit on COMBI particle distribution, assuming a double Gaussian profile, integrating numerically over COMBI particle distribution and taking into account the change of β at the IP respectively. A transverse feedback is activated on both beams.

The blue curve assumes the beam distribution to be Gaussian (Eq. 2) with the input RMS beam size meaning β^* remains unchanged, which is expected to be accurate for small

values of the beam-beam parameter, as the dynamic β effect is small. The luminosity increases as ξ_{bb}^2 as expected.

The second way of computing the luminosity (green curve) assumes a Gaussian distribution of the bunch (Eq. 2) but takes into account the bunch distribution generated by COMBI. For a given ξ_{bb}, a value of the bunch size $\sigma_{x,y}$ was deduced from the Gaussian fit on both planes with least square method. The results provided by this method are similar to the previous case until $\xi_{bb} \approx 0.075$, the increase as a function of the beam-beam parameter is then smaller than the square of intensity N^2. This deviation hints towards a possible alteration in the bunch distribution with respect to Gaussian distribution profiles.

The most accurate way of luminosity computation consists in integrating numerically the bunch distribution generated by COMBI using Eq. 11 (light blue curve). In the latter case, the deviation from the unperturbed σ case appears for a beam-beam parameter slightly larger ($\xi_{bb} \gtrapprox 0.08$). The results provided by numerical integration are always close to the assumption that the bunch has a double Gaussian distribution (red curve). This indicates that the double Gaussian profile assumption is always a good approximation, whatever the value of the beam-beam parameter is.

The Gaussian curve taking into account the change in β at the IP (purple curve) always predicts a gain in luminosity compared to an unchanged distribution (blue). This means that the beam size, and thus the β^*, decrease after collision. However, the bunch is composed of particles with various amplitudes such that this curve corresponds to an upper limit of the luminosity. Indeed, as the amplitude of the particle increases, the change in the β-function decreases and converges to zero for very large amplitude [43]. Therefore, for very large amplitude particles, the beam size does not change and the value of the luminosity converges to the one of the unchanged Gaussian distribution (blue curve). This is why the computation of the luminosity should be in between these two curves (blue and purple) when the Gaussian distribution assumption is correct, which is the case until $\xi_{bb} \sim 0.07$. Above this value, the assumptions from Eq. 4 are not valid anymore (large ξ_{bb}, deviation from Gaussian distribution). For $\xi_{bb} \approx 0.11$, one reaches a 20% deviation between the analytical luminosity with the Gaussian assumption (between blue and purple) and the luminosity computed numerically from COMBI distribution (light blue).

An illustration of the deviation of the bunch profile with respect to a Gaussian distribution is presented in Fig. 22 for a large beam-beam parameter ($\xi_{bb} = 0.0916$). A Gaussian and double Gaussian fit are drawn based on the bunch profiles (black and blue curve respectively).

The bunch distribution in the vertical plane (Fig. 22b) is close to a Gaussian. However, in the horizontal plane (Fig. 22a), the Gaussian fit does not represent accurately the distribution. Concerning the double Gaussian fits, they match more accurately the bunch distribution, even for a large beam-beam parameter, which is more prominent on the horizontal plane. The longitudinal profile was always well represented by a Gaussian distribution, whatever the beam-beam parameter was as expected since there is no force

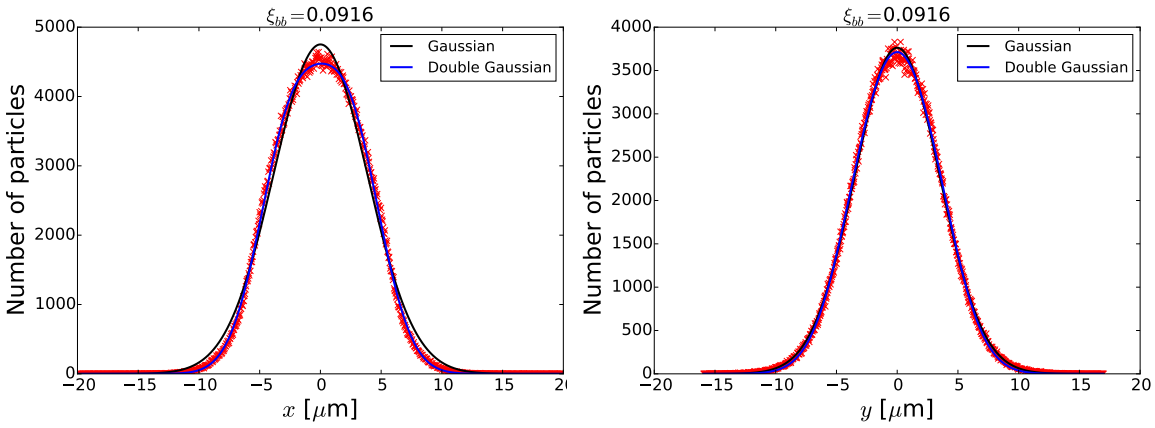

(a) Horizontal plane

(b) Vertical plane

Figure 22: Particle distribution from COMBI simulations with $5 \cdot 10^6$ macroparticles per bunch after 10^5 turns

along this axis. Thus, a large beam-beam parameter ($\xi_{bb} \gtrapprox 0.075$) has a negligible influence on the longitudinal and vertical plane but a non-negligible one on the horizontal one.

6.2 Transverse feedback off

COMBI simulations without transverse feedback on the beams are now presented. The related luminosity scan as a function of beam-beam parameter ξ_{bb} is presented in Fig. 23 where the same five ways of computing the luminosity were used.

The blue curve from Fig. 23 corresponds to Eq. 2 with constant Gaussian beam size and the purple one adds the dynamic β effect of the zero amplitude particles as previously (Eq. 4). These two curves remain the same as in the previous scan. Concerning the other methods (based on generated COMBI distributions), the three of them are between the blue and purple curves as before until $\xi_{bb} \gtrapprox 0.075$. For a larger beam-beam parameter, the curves based on COMBI output deviate from the two previous analytical expressions. The absence of transverse feedback on the beams makes the luminosity increase not continuous compared to the case with transverse feedback.

An illustration of the deviation of the bunch profile with respect to a Gaussian distribution is presented in Fig. 24 for a beam-beam parameter $\xi_{bb} = 0.0749$. A Gaussian and double Gaussian fit are drawn based on the bunch profiles (black and blue curve respectively).

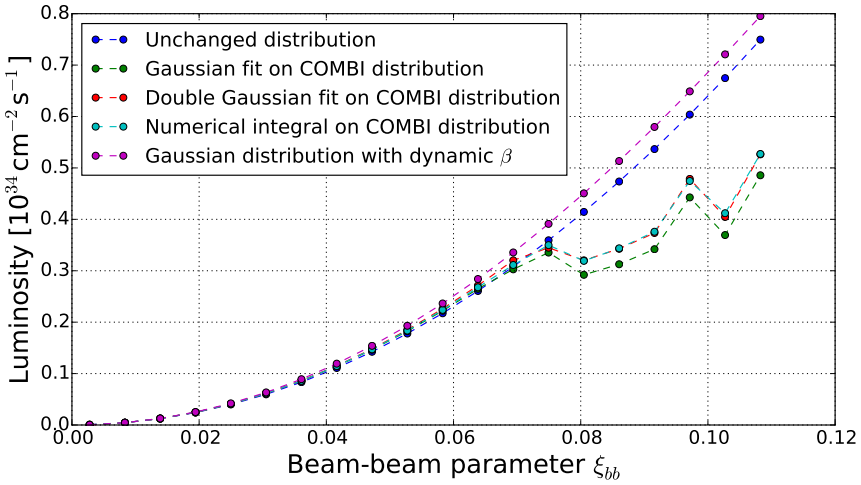

Figure 23: Luminosity as a function of the beam-beam parameter ξ_{bb}. The blue, green and red curves correspond to the luminosity computed assuming a Gaussian particle distribution (Eq. 11) with the input RMS beam sizes, with RMS beam size derived using a Gaussian fit on COMBI particle distribution and integrating numerically over COMBI particle distribution respectively. No transverse feedback is used.

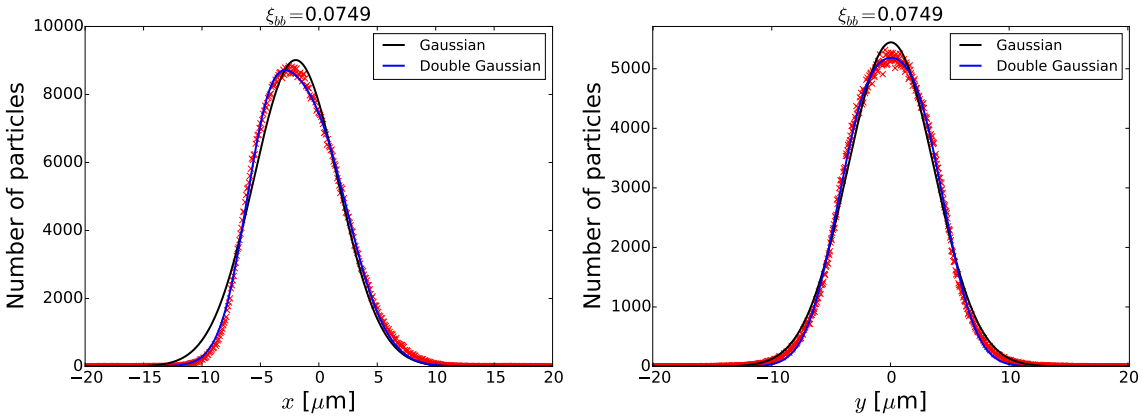

(a) Horizontal plane

(b) Vertical plane

Figure 24: Particle distribution from COMBI simulations with $5 \cdot 10^6$ macroparticles per bunch after 10^5 turns

In this case, given that there is no transverse feedback, coherent beam-beam modes are excited and the tilt we observe is due to the presence of a π-mode with a non-negligible amplitude. Indeed, the two bunches being opposed in phase space, the offset between them at the IP, and therefore the beam-beam force, is different every turn. Thus, the bunch distribution will change according to the turn we are looking at [45]. In order to compute properly the luminosity in this case, the average bunch distribution over multiple turns should be taken into account. The results should then be similar to the case with a transverse damper as in the Sec. 6.1.

7 Beam-beam impact on the FCC-hh collimation system

LHC, HL-LHC and FCC-hh will be both equipped with a very efficient multistage collimation to control losses. The aim of such a system is to protect the delicate elements of the machine, to help reduce the total dose on the accelerator equipment and to optimize the background for the experiments. It ensures in particular that the beam losses in superconducting magnets remain below quench limits. Specific insertions in the machine are dedicated to the cleaning of the beams due to large transverse excursions (betatron collimation) or large energy offset (momentum collimation). This cleaning stage is achieved by placing very precisely blocks of materials close to the circulating beams, while respecting a pre-defined collimator hierarchy to ensures optimum cleaning in the multi-stage collimation process (Fig. 25) : primary and secondary collimators are the devices closest to the circulating beam that perform most of the cleaning process, then at larger apertures the shower absorbers and tertiary collimators complete the system [46].

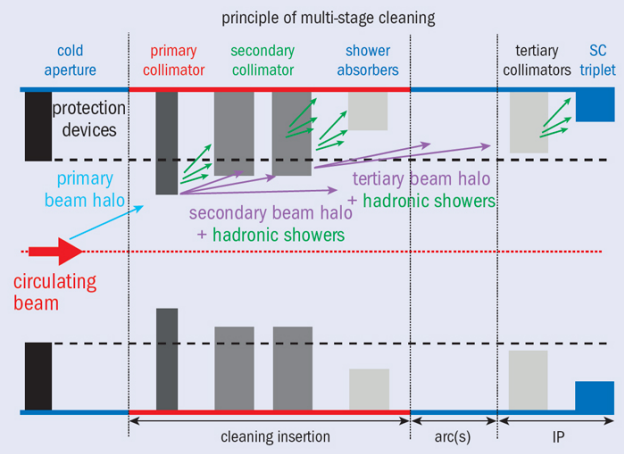

Figure 25: Illustration of multi-stage betatron collimation system. Primary collimators intercept protons lost from the beam core. Secondary collimators and absorbers intercept halo protons and hadronic showers produced by particles interacting with the collimator jaws. Tertiary collimators ensure further protection near the experiments [46].

The collimation hierarchy and therefore the cleaning efficiency is very sensitive to the machine optics, in particular to the β-function and the phase advance between collimators. This is why the position of the collimators and the margins associated to the change of the β-function are crucial to ensure the safety of the elements.

At nominal energy, the energy stored in each beam in the FCC-hh is planned to be 8.4 GJ, i.e. more than 20 times the one in the LHC and 10 times the HL-LHC [47]. Thus, extremely efficient collimation is required in order to prevent uncontrolled beam losses in the superconducting magnets and a magnet quench. Due to the difference in stored energy, the limit of beam losses in cold magnets is significantly smaller in the FCC-hh in comparison to the LHC ($7.6 \cdot 10^6$ particles $\cdot\, \mathrm{s}^{-1} \cdot \mathrm{m}^{-1}$ in the LHC [48] against $0.5 \cdot 10^6$ particles $\cdot\, \mathrm{s}^{-1} \cdot \mathrm{m}^{-1}$ in the FCC-hh [49]). In this new scenario, it is extremely

important to evaluate the impact of the optics distortion due to the beam-beam interaction.

For the results presented next, the latest FCC-hh optics are used. Only the betatron collimation system with primaries and secondaries is considered. The aperture will be calculated using the `APERTURE` command in MADX, where the halo parameter is set such that the N_1 parameter corresponds to the actual aperture in σ. This command allows to include additional parameters like β-beating and closed orbit errors among others. The values assumed at this moment are similar to the LHC case [48].

The intensity is scanned to evaluate the impact of the head-on only in two experiments (HO) on the machine aperture (Fig. 26a). The bottleneck, i.e. the smallest transverse aperture at any location around the ring, is at the dipole MBRD.B4RA.H1 ($s = 92398.2$ m) with a focusing effect that enlarges the aperture at that location with increasing beam-beam parameter until a maximum of 16.22 σ. After a beam-beam parameter $\xi_{bb} \sim 0.08$, the bottleneck changes to the dipole MBRD.B4RG.H1 ($s = 43523.2$ m) and the aperture decreases.

If we now do the same exercise including as well the long-range interactions in both IPs (HO+LR), the bottleneck remains first at the dipole MBRD.B4RA.H1 and then changes to MBRD.B4RG.H1 again (Fig. 26a). The transition occurs at a larger beam-beam parameter ($\xi_{bb} \gtrapprox 0.093$). In this case, the effect is defocussing at first reaching a minimum of 14.75 σ, increasing afterwards and finally, when changing bottleneck, defocussing again.

Fig. 27 presents the machine aperture of the FCC-hh for different beam-beam parameters below 20 σ. The minimum aperture for $\xi_{bb} = 0.03$ is around 14.75 σ implying a decrease of 0.25 σ.

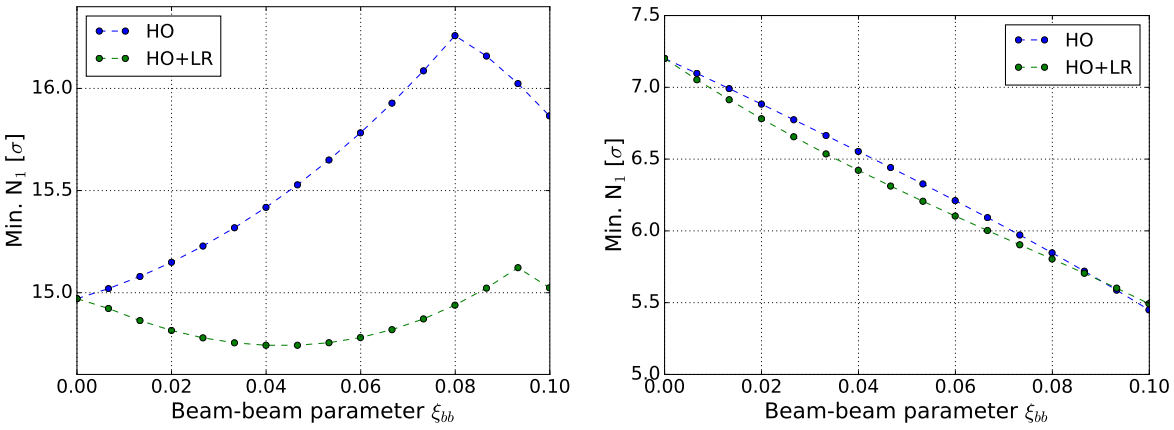

(a) Machine aperture

(b) Collimator aperture (primary and secondary)

Figure 26: Minimum of N_1 as a function of the beam-beam parameter ξ_{bb}

The collimators are movable objects that can be adjusted dynamically during the operation cycle to better handle the losses. However, it is assumed next that from the moment the collision starts with the collimators at nominal aperture, there is a period where the aperture will be modified before the collimators will be placed at newer apertures. In

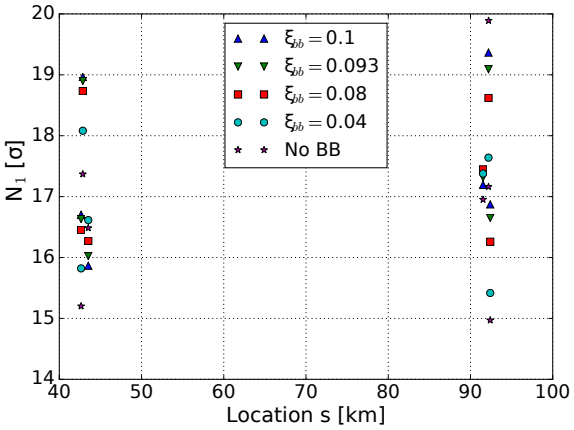

(a) Machine aperture distortion with only HO at two IPs

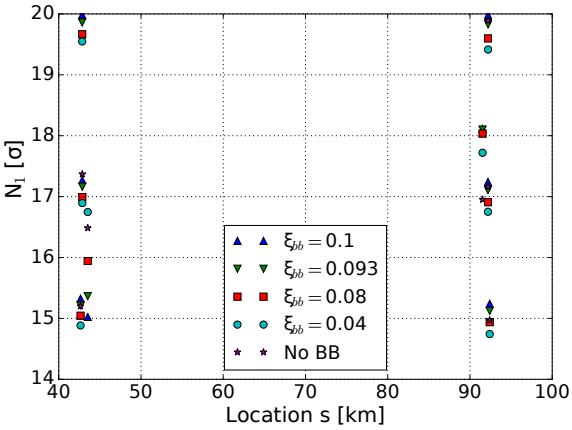

(b) Machine aperture distortion with HO and LRs at two IPs

Figure 27: N_1 as a function of the location s for different beam-beam parameters

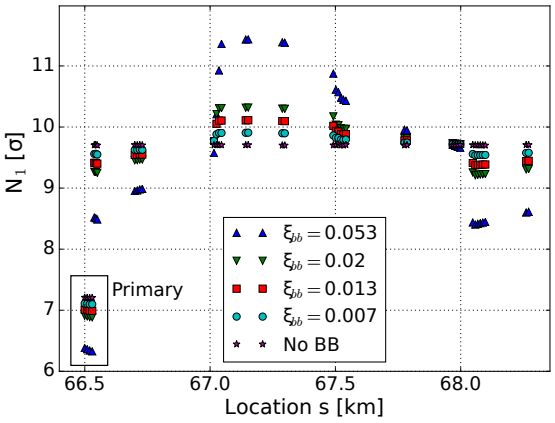

(a) Collimators aperture distortion with only HO at two IPs

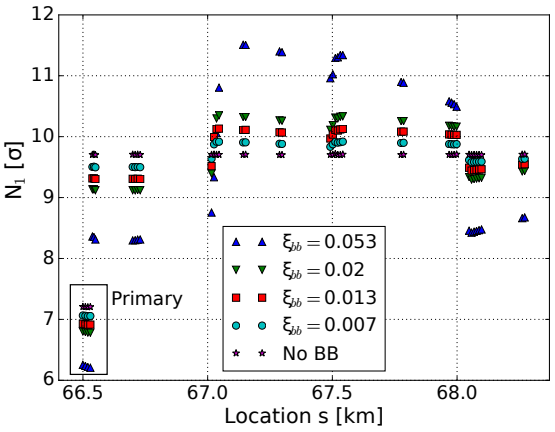

(b) Collimators aperture distortion with HO and LRs at two IPs

Figure 28: N_1 as a function of the location s for different beam-beam parameters

Fig. 26b, the apertures of the collimators as a function of ξ_{bb} is shown. The bottleneck is first the TCP.B6L2.B1 at $s = 66519.7$ m and then becomes the TCP.A6L2.B1 at $s = 66529.7$ m. The transition between the two bottlenecks occurs for $\xi_{bb} \approx 0.01$ and $\xi_{bb} \approx 0.016$ for head-on and head-on with long-ranges interactions, respectively.

Fig. 28 presents the collimator aperture of the FCC-hh for different beam-beam parameters below 12 σ. The minimum aperture for $\xi_{bb} = 0.03$ is around 6.5 σ implying a decrease of almost 1 σ.

From the previous results, the machine aperture is not significantly affected by the expected β-beating due to beam-beam. On the other hand, the aperture of the collimators is significantly decreased for the nominal ultimate $\xi_{bb} = 0.03$, although no changes in the hierarchy is observed. This would require that the collimators should be further opened just before the collision starts to account for this effect and ensure 7.5 σ. Since the β-function and thus the β-beating are amplitude dependent [43, 50], so is this effect. However, it is not taken into account by the N_1 factor. Similar studies should be performed to ensure similar corrections for the LHC and HL-LHC.

8 Conclusion

In this study, we analytically, numerically and experimentally explored the impact of orbit distorsions, β-beating due to beam-beam effects, on the particle detuning with amplitude, luminosity and collimation.

The agreement between the beam-beam amplitude detuning formulas including free and forced oscillations and single particle simulations from COMBI has been shown, probing the validity of the analytical expressions in weak-strong regimes. COMBI demonstrated its importance as a tool to simulate the real beam-beam dynamics in different scenarios : with and without damper, offset, different intensities and emittances. In this case, a deviation was observed between the multi-particle simulation and the analytical expressions, however, both converged as the collective effects between the beams were suppressed as expected.

For the first time, a measurement of the β-beating due to beam-beam was successfully done in a hadron collider and a good agreement with simulations was demonstrated. Some challenges in identifying the best natural tune still persist : while the RMS β-beating provided consistent results, issues were encountered with the two other methods, especially the phase advance method.

For future measurements, forced oscillations should be made in one plane in order to be able to compare the measured spectra from the experiment to the analytical expressions presented in this work. A greater emittance should also be chosen to avoid the uncertainty from the BSRT system and strong excitation amplitudes should be aimed given that only the strongest AC dipole excitation provided a natural tune that led to the consistent β-beating measurement.

Additional implications for the luminosity have been studied like the range of validity of the Gaussian bunch distribution assumption where COMBI simulations showed that for $\xi_{bb} \gtrapprox 0.07$, the beam-beam force has a non-negligible impact on the luminosity computation that can reach about 20% for $\xi_{bb} \sim 0.11$. The increase in luminosity coming from the dynamic β^* was consistent with the computed luminosity for smaller beam-beam parameters. The role of the transverse damper to avoid dynamic variations of the beam distribution due to the π-mode was shown.

Finally, apertures and collimation system implications were evaluated scanning the beam-beam parameter including head-on and head-on with long-range interactions. The expected β-beating from beam-beam does not affect significantly the machine aperture. However, the aperture of the collimators is significantly decreased by $\sim 1\ \sigma$ for the scenario with $\xi_{bb} = 0.03$. A change in the bottleneck location as a function of the beam-beam parameter was always witnessed. Concerning the machine aperture, the effect on the minimum aperture changed at that transition (focusing/defocussing). With the primary and secondary collimators installed, the effect remained defocussing and no changes in the hierarchy was observed. The effect of the beam tail, i.e. particles oscillating with a large amplitude, remain to be studied. Similar effects should be expected for the HL-LHC since

a beam-beam parameter of similar amplitude is expected.

9 References

[1] "MD979: Beta-beating correction on colliding beams", CERN-ATS-Note, to be published.

[2] P. Gonçalves Jorge *et al.*, "Measurement of beta-beating due to strong head-on beam-beam interaction in the LHC", in *Proc. of IPAC'17*, Copenhagen, Denmark, May 2017, paper TUPVA030, pp.2121-2124.

[3] R. Tomás, X.Buffat, S. White, J. Barranco, P. Gonçalves Jorge, T. Pieloni, "Beam-beam amplitude detuning with forced oscillations", Jul. 2017, to be published.

[4] W. Herr, "Beam-beam interactions", CAS - CERN Accelerator School : Intermediate Course on Accelerator Physics, CERN-2006-002, Geneva, Switzerland, 2006.

[5] Widemann Helmut, "Particle accelerator physics", fourth edition, Springer, Berlin, 2015.

[6] Large Hadron Collider CERN webpage, https://home.cern/topics/large-hadron-collider, last accessed 17 July 2017.

[7] Future Circular Collider CERN webpage, https://home.cern/about/accelerators/future-circular-collider, last accessed 17 July 2017.

[8] High Luminosity Large Hadron Collider CERN webpage, http://hilumilhc.web.cern.ch/, last accessed 17 July 2017.

[9] Nature journal, "Building a behemoth", http://www.nature.com/nature/journal/v448/n7151/full/nature06077.html, last accessed 2 July 2017.

[10] FCC-hh baseline layout and parameter, CERN webpage, https://fcc.web.cern.ch/Pages/news/FCC-hh-baseline-layout-and-parameter.aspx, last accessed 16 July 2017.

[11] D. Sagan, "The dynamic beta effect in CESR", in *16th Biennial Particle Accelerator Conference*, Dallas, USA, 1995.

[12] D. Brandt *et al.*, "Is LEP beam-beam limited at its highest energy?", in *Proc. Particle Accelerator Conf.*, New York, USA, 1999, p. 3005, http://dx.doi.org/10.1109/pac.1999.792127.

[13] P. M. Ivanov *et al.*, "Experimental studies of beam-beam effects at VEPP-2M", in *Proc. Workshop on beam-beam effects in circular colliders*, Fermilab, p. 36 (2001).

[14] D. Cinabro *et al.*, "Observation of the dynamic beta effect at CESR with CLEO", CLNS 97/1496. CLEO CONF 97-11. EPS Abstract 356 (1998).

[15] M. Bai *et al.*, "Considerations for an AC dipole for the LHC", in *Proc. of the 22nd Particle Accelerator Conf.*, Albuquerque, New Mexico, USA, 2007.

[16] D. Boussard, T. Linnecar, W. Höfle, "The LHC transverse damper (ADT) performance specification", CERN, Geneva, Switzerland, Rep. SL-Note-99-055-HRF, 1999, http://cdsweb.cern.ch/record/702559, last accessed 17 June 2017.

[17] MAD-X CERN website, http://madx.web.cern.ch/madx/, last accessed 07 July 2017.

[18] Karl L. Brown, "A first- and second-order matrix theory for the design of beam transport systems and charged particle spectrometers", Stanford linear accelerator center, Stanford, 1982.

[19] H. Grote and F. C. Iselin, "The MAD program (Methodical Accelerator Design)", CERN/SL/90-13(AP), 1991, Geneva, Switzerland.

[20] P. Gonçalves Jorge, "Computation of linear optics distortions due to head-on beam-beam interactions in hadron colliders", CERN-THESIS-2015-404.

[21] COMBI website, http://lhc-beam-beam.web.cern.ch/lhc-beam-beam/combi_welcome.html, last accessed 17 July 2017.

[22] T. Pieloni, "A study of beam-beam effects in hadron colliders with a large number of bunches", PhD thesis from EPFL, Lausanne, Switzerland, 2008.

[23] X. Buffat, "Transverse beams stability studies at the Large Hadron Collider", PhD thesis from EPFL, Lausanne, Switzerland, 2015.

[24] R. Tomás, "Adiabaticity of the ramping process of an AC dipole", *Phys. Rev. ST Accel. Beams*, Vol. 8, 024401, 2005.

[25] Y. Alexahin, "A study of the coherent beam-beam effect in the framework of the Vlasov perturbation theory", Nucl. Instrum. Methods Phys. Res. A 480, 253, 2002.

[26] Y. Alexahin, W. Herr, H. Grote, M. P. Zorzano, "Coherent beam-beam effects in the LHC", LHC Project Report 469, 2001, presented at HEACC01.

[27] W. Herr, M. P. Zorzano, and F. Jones, "Hybrid fast multipole method applied to beam-beam collisions in the strong-strong regime", *Phys. Rev. ST Accel. Beamsv4*, 054402, 2001.

[28] W. Hofle, "Transverse feedback systems in LHC and its injectors: projected performance and upgrade paths", 3rd CARE-HHH-APD Workshop, LHC-Lumi-06, Valencia, 16-20 October 2006, CERN-2007-002 (2007) 177-179.

[29] J.-P. Burnet, "Requirements for power converters", CERN-2015-003.

[30] J. Qiang, J. Barranco, T. Pieloni and K. Ohmi, "Beam-beam simulation of crab cavity white noise for LHC upgrade", in *Proc. of IPAC'15*, S. Henderson *et al.* eds., (2015), pg. 2206.

[31] R. Tomás, "Normal form of particle motion under the influence of an AC dipole", *Phys. Rev. ST Accel. Beams*, volume 5 54001, 2002.

[32] R. Miyamoto, S. E. Kopp, A. Jansson, and M. J. Syphers, "Parametrization of the driven betatron oscillation", *Phys. Rev. ST Accel. Beams 11*, 084002, 2008.

[33] A. Hofmann, "Landau damping", CAS - CERN Accelerator School : Intermediate Course on Accelerator Physics, Zeuthen, Germany, 2003, ed. by D.Brandt, CERN-2006-002, pp.271-304.

[34] L. Medina, R. Tomás, X. Buffat, J. Barranco, and T. Pieloni, "Correction of beta-beating due to beam-beam for LHC and its impact on dynamic aperture", in *Proc. of IPAC'17*, Copenhagen, Denmark, May 2017, paper WEOAB2, pp. 2512-2515.

[35] G. Trad et al., "Performance of the upgraded synchrotron radiation diagnostics at the LHC", in *Proc. of IPAC'16*, Busan, Korea, May 2016, paper MOPMR030, pp. 1403-1406.

[36] G. Trad, private communication, Mar. 2017.

[37] R. J. Steinhagen *et al.*, "Advancements in the base-band-tune and chromaticity instrumentation and diagnostics systems during LHCs first year of operation", CERN, Geneva, Switzerland, Rep. CERN-BE-2011-016, 2011.

[38] A. Langner *et al.*, "Utilizing the N beam position monitor method for turn-by-turn optics measurements", *Phys. Rev. Accel. Beams*, Vol. 19, 092803, 2016.

[39] R. Miyamoto, "Diagnostics of the Fermilab Tevatron using an AC dipole", Ph.D. thesis, Texas University, USA, 2008.

[40] M. Aiba *et al.*, "First β-beating measurement and optics analysis for the CERN Large Hadron Collider", *Phys. Rev. ST Accel. Beams*, Vol. 12, 081002, 2009.

[41] R. Tomás *et al.*, "CERN Large Hadron Collider optics model, measurements, and corrections", *Phys. Rev. ST Accel. Beams*, Vol. 13, 121004, 2010.

[42] F. Carlier, "RDTs from Beam-Beam at Injection Energy in the LHC", https://indico.cern.ch/event/645084/contributions/2619193/attachments/1474023/2282101/pres.pdf, last accessed 01 July 2017.

[43] P. Gonçalves Jorge, "Computation of optics distortions due to beam-beam interactions in the FCC-hh", CERN-THESIS-2016-317.

[44] W. Herr, B. Muratori, "Concept of luminosity", in *Proc. of CERN Accelerator School*, CERN-2006-002, 2003.

[45] X. Buffat, "Intensity limitations in particle beams - coherent beam-beam effects", https://indico.cern.ch/event/362960/contributions/1776150/attachments/1179168/1713104/presentation-expanded.pdf, last accessed 07 July 2017.

[46] S. Redaeli *et al.*, "Cleaning insertions and collimation challenges", CERN, 2015, https://cds.cern.ch/record/2131745/files/Cleaning%20Insertions%20and%20Collimation%20Challenges.pdf, last accessed 15 July 2017.

[47] R. Bruce *et al.*, "collimator layouts for HL-LHC in the experimental insertions", in *Proc. of IPAC'15*, Richmond VA, USA, May 2015, paper TUPTY028, pp.2064-2067.

[48] G. Valentino *et al.*, "Comparison of Beam Sizes at the Collimator Locations from Measured Optics and Beam-based Collimator Alignment in the LHC", in *Proc. of IPAC'15*, Richmond VA, USA, May 2015, paper TUPTY040, pp.2101-2104.

[49] A. Langner *et al.*, "Betatron collimation system insertion", FCC Week, 30.05.2017, https://indico.cern.ch/event/556692/contributions/2484254/attachments/1467177/2268615/talk_alangner.pdf, last accessed 10 July 2017.

[50] T. Pieloni *et al.*, "Dynamic beta and beta-beating effects in the presence of the beam-beam interactions", in *Proc. of HB2016*, Malmo, Sweden, Jul. 2016, paper MOPR027, pp. 136-139.

Appendices

A Intensity plots from MD 979

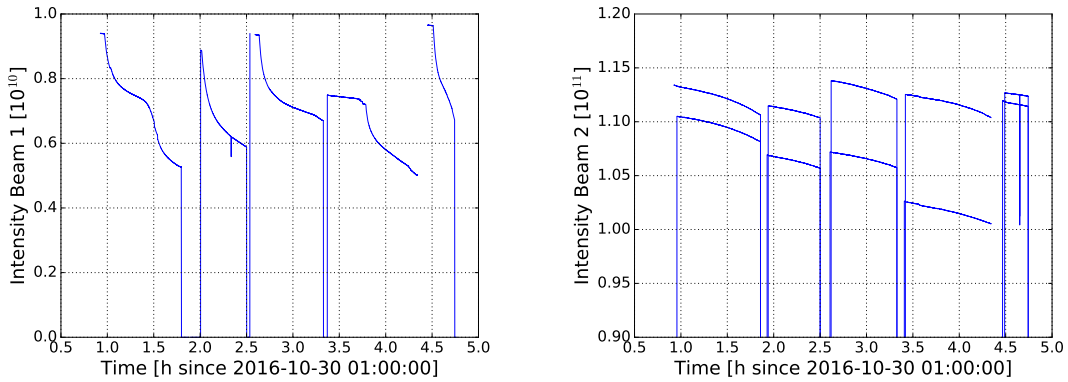

(a) Beam 1

(b) Beam 2

Figure 29: Intensity of colliding bunches of both beams as a function of time during the second period of the MD

B Emittances plots from MD 979

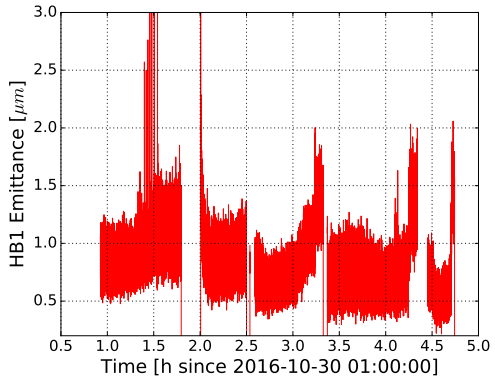

(a) Horizontal normalized emittance of beam 1

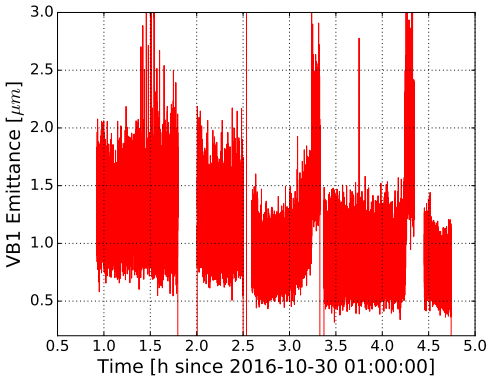

(b) Vertical normalized emittance of beam 1

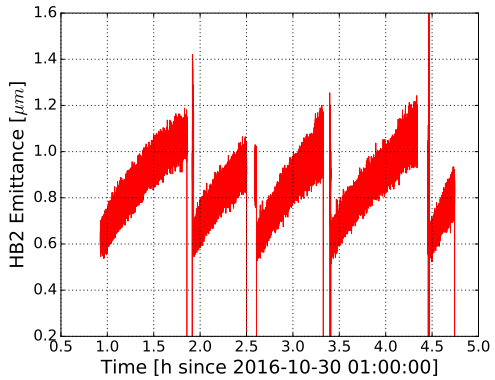

(c) Horizontal normalized emittance of beam 2

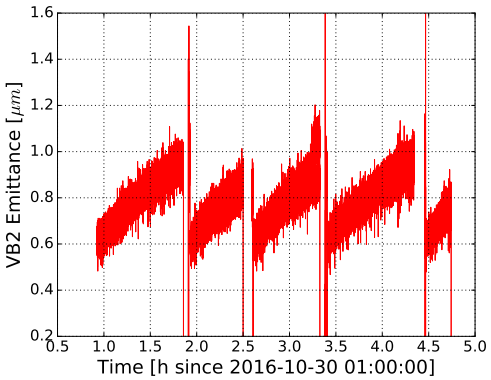

(d) Vertical normalized emittance of beam 2

Figure 30: Normalized emittances of beam 1 and 2 from BSRT measurements as a function of time during the second period of the MD